



Chlorinated ethene plume evolution after source thermal remediation: Determination of degradation rates and mechanisms



Alexandra Marie Murray^{a,*}, Cecilie B. Ottosen^a, Julien Maillard^b, Christof Holliger^b, Anders Johansen^c, Lærke Brabæk^a, Inge Lise Kristensen^a, Jeremy Zimmermann^d, Daniel Hunkeler^d, Mette M. Broholm^a

^a Department of Environmental Engineering, Technical University of Denmark, Kgs. Lyngby DK-2800, Denmark

^b Laboratory for Environmental Biotechnology, ENAC-IIE, Ecole Polytechnique Fédérale de Lausanne, 1015 Lausanne, Switzerland

^c Department of Environmental Science, Aarhus University, Frederiksborgvej 399, 4000 Roskilde, Denmark

^d Centre for Hydrogeology & Geothermics (CHYN), University of Neuchâtel, Rue Emile Argand 11, CH 2000 Neuchâtel, Switzerland

ARTICLE INFO

Keywords:

Stable isotopes
Molecular biology
Dehalogenimonas spp.
Biodegradation
Abiotic degradation
Multiple lines of evidence

ABSTRACT

The extent, mechanism(s), and rate of chlorinated ethene degradation in a large tetrachloroethene (PCE) plume were investigated in an extensive sampling campaign. Multiple lines of evidence for this degradation were explored, including compound-specific isotope analysis (CSIA), dual C-Cl isotope analysis, and quantitative real-time polymerase chain reaction (qPCR) analysis targeting the genera *Dehalococcoides* and *Dehalogenimonas* and the genes *vcrA*, *bvcA*, and *cerA*. A decade prior to this sampling campaign, the plume source was thermally remediated by steam injection. This released dissolved organic carbon (DOC) that stimulated microbial activity and created reduced conditions within the plume. Based on an inclusive analysis of minor and major sampling campaigns since the initial site characterization, it was estimated that reduced conditions peaked 4 years after the remediation event. At the time of this study, 11 years after the remediation event, the redox conditions in the aquifer are returning to their original state. However, the DOC released from the remediated source zone matches levels measured 3 years prior and plume conditions are still suitable for biotic reductive dechlorination. *Dehalococcoides* spp., *Dehalogenimonas* spp., and *vcrA*, *bvcA*, and *cerA* reductive dehalogenase genes were detected close to the source, and suggest that complete, biotic PCE degradation occurs here. Further downgradient, qPCR analysis and enriched $\delta^{13}\text{C}$ values for *cis*-dichloroethene (cDCE) suggest that cDCE is biodegraded in a sulfate-reducing zone in the plume. In the most downgradient portion of the plume, lower levels of specific degraders supported by dual C-Cl analysis indicate that the biodegradation occurs in combination with abiotic degradation. Additionally, 16S rRNA gene amplicon sequencing shows that organizational taxonomic units known to contain organohalide-respiring bacteria are relatively abundant throughout the plume. Hydraulic conductivity testing was also conducted, and local degradation rates for PCE and cDCE were determined at various locations throughout the plume. PCE degradation rates from sampling campaigns after the thermal remediation event range from 0.11 to 0.35 yr⁻¹. PCE and cDCE degradation rates from the second to the third sampling campaigns ranged from 0.08 to 0.10 yr⁻¹ and 0.01 to 0.07 yr⁻¹, respectively. This is consistent with cDCE as the dominant daughter product in the majority of the plume and cDCE degradation as the time-limiting step. The extensive temporal and spatial analysis allowed for tracking the evolution of the plume and the lasting impact of the source remediation and illustrates that the multiple lines of evidence approach is essential to elucidate the primary degradation mechanisms in a plume of such size and complexity.

1. Introduction

Chlorinated ethenes such as tetrachloroethene (PCE) are toxic pollutants commonly found in groundwater. Because chlorinated ethenes can be transported with groundwater over long distances and deep into

aquifers, remediation is challenging. Natural attenuation is preferred whenever possible, and other intensive methods, such as thermal remediation, are used to remove chlorinated ethenes in plume source zones where the concentration is highest (Friis et al., 2005). Thermal remediation by steam enhanced extraction releases dissolved organic

* Corresponding author.

E-mail address: almu@env.dtu.dk (A.M. Murray).

<https://doi.org/10.1016/j.jconhyd.2019.103551>

Received 7 March 2019; Received in revised form 28 August 2019; Accepted 30 August 2019

Available online 02 September 2019

0169-7722/ © 2019 Elsevier B.V. All rights reserved.

carbon (DOC) from the soil and aquifer material. The released DOC promotes microbial activity downgradient from the remediation site and can stimulate chlorinated ethene degradation by organohalide-respiring bacteria (OHRB) without additional engineering intervention; e.g. via biostimulation or bioaugmentation (Badin et al., 2016; Friis et al., 2005).

Just like naturally occurring SO_4^{2-} and Fe(III), chlorinated ethenes can serve as electron acceptors in the subsurface (Holliger et al., 1993). The use of PCE as an electron acceptor by OHRB sequentially yields trichloroethene (TCE), *cis*-dichloroethene (cDCE), vinyl chloride (VC), and ultimately the harmless ethene. More reduced conditions are needed as the chlorinated ethenes become further degraded, and it is not uncommon for degradation of these compounds to slow or halt partway through the sequence and cause accumulation of cDCE and potentially the daughter product VC (Bradley, 2000; Shani et al., 2013). Degradation of these contaminants is also dependent on the presence of electron donors, typically H_2 , and the presence of bacteria capable of chlorinated ethene degradation. OHRB represent various bacterial genera, such as *Sulfurospirillum*, *Dehalobacter*, *Desulfitobacterium*, and *Desulfuromonas*, but these OHRB can only facilitate degradation to cDCE (Hug et al., 2013). Until recently, only the genus *Dehalococcoides* was identified as capable of degrading cDCE and VC to ethene via the VC dehalogenases VcrA and BvcA (Löffler et al., 2013; Yargicoglu and Reddy, 2015), though it had been posited that other as yet unidentified bacteria may also possess the capability (Maphosa et al., 2010). Recently, the genus *Dehalogenimonas* was identified as capable of VC reduction to ethene via the VC dehalogenase CerA (Yang et al., 2017). This discovery has shifted the paradigm that complete biotic degradation of chlorinated ethenes is only possible when *Dehalococcoides* is a main player in a groundwater microbial community. Further, it is also possible for cDCE and VC to be degraded by microbial oxidation, including microaerophilic oxidation, cometabolic oxidation by methanotrophs and ethenotrophs, or anaerobic oxidation (Bradley et al., 1998; Bradley and Chapelle, 2000; Liang et al., 2017; Smits et al., 2011). Chlorinated ethene degradation may also proceed abiotically in iron- and sulfate-reducing conditions when mediated by reactive iron minerals such as iron sulfides, magnetite, and green rust (He et al., 2015). For instance, the iron sulfide mineral pyrite is capable of degrading all chlorinated ethene compounds via β -elimination, where the main product is acetylene (Lee and Batchelor, 2002a).

It is recommended for risk management of monitored natural attenuation to assess the extent, mechanism, and rate of degradation of chlorinated ethenes in the subsurface (Yargicoglu and Reddy, 2015) in what can be called the multiple lines of evidence approach. In this approach, various analyses are used in combination to yield a comprehensive picture of the state of a contaminant plume (Wilson, 2010), and it has been used successfully over the past decade (Courbet et al., 2011; Damgaard et al., 2013; Imfeld et al., 2008; Nijenhuis et al., 2007). New chemical and biological tools are available that can aid in this endeavor. One such tool is compound specific isotopic analysis (CSIA), which has been used over the last decades to determine in situ degradation of chlorinated ethenes (Braeckevelt et al., 2012). Additionally, dual C-Cl analysis can assist in distinguishing between degradation pathways (Elsner et al., 2012). The database of laboratory determined C-Cl isotope slopes has continued to expand in recent years, though there are still limitations that render this method best used along with other lines of evidence (Badin et al., 2016; Doğan-Subaşı et al., 2017; Gafni et al., 2018). Bio-molecular approaches can also assist in assessing the likelihood that biotic degradation occurs. Quantitative real-time polymerase chain reaction (qPCR) analyses can be used to identify whether specific genera and reductive dehalogenase (*rdhA*) genes are present in the plume, and Illumina sequencing analysis can be used to screen the entire microbial community (Imfeld et al., 2011; Paes et al., 2015; Yargicoglu and Reddy, 2015). Moreover, when the mechanism and extent of degradation are quantified and combined with knowledge of the aquifer hydrogeology, the rate of degradation

can be estimated. This is essential knowledge for accurate risk assessment of a polluted site – yet few of the rates published in the literature are determined at the field scale, and for chlorinated ethenes, published rates span multiple orders of magnitude (Ottosen et al., 2019).

The aim of the current study is to use the new tools and knowledge available, including knowledge about *Dehalogenimonas* spp. and dual C-Cl isotope analysis, to investigate the degradation mechanism(s) that occur in a chlorinated ethene plume and to quantify the rate at which degradation proceeds. Furthermore, we aim to assess the long-term impact of source thermal remediation on a chlorinated ethene plume. Use of the multiple lines of evidence approach is essential because little VC is measured in the plume, and thus the fate of cDCE is unclear (Damgaard et al., 2013). The new tools can in particular advance our understanding of the fate of cDCE.

Two previous comprehensive sampling campaigns have been conducted on the plume, one prior to thermal remediation and one 8 years later. The current study has been carried out 11 years post-remediation. A comprehensive sampling campaign was conducted that involved measurement of hydraulic conductivity, redox parameters, and chlorinated ethene concentrations and isotopic composition; qPCR analysis of selected OHRB and VC *rdhA* genes, including the newly reported *cerA*; and bacterial community analysis by 16S rRNA gene amplicon sequencing. This extensive characterization of the Rødekro plume, through time and with numerous lines of evidence, allows for both localized and broad interpretation of the degradation mechanisms that occur throughout the plume. In this study, we first present each line of evidence and its interpretation individually and then discuss process understanding of each section of the plume based on review of all lines of evidence. We conclude by evaluating the spatial and temporal evolution of the plume as a whole and give some prospective remarks as to possible further development.

2. Study site description

The study site is located in the town of Rødekro, in southern Denmark, and has previously been described by Hunkeler et al. (2011) and Badin et al. (2016). A dry-cleaning facility was in operation at the site from 1964 to 2001 and is the origin of the PCE contamination. The subsurface material is primarily sand, interspersed with gravel and clay lenses (Hunkeler et al., 2011). A PCE plume originates from the decommissioned dry-cleaning facility and extends ~2 km downgradient toward the south; after 1 km the plume bends slightly toward the southeast, in accordance with the flowfield depicted in Fig. 1.

Thermal remediation via steam injection was conducted at the source zone in 2006, which effectively removed the main dense non-aqueous phase liquid source. The initial state of the plume is presented in Hunkeler et al. (2011), and the effect of the thermal remediation event after 8 years, in 2014, is described by (Badin et al., 2016). Chlorinated ethene concentrations measured in the plume from close to the source zone to 750 m from the source were 85% lower in 2014 than in 2006. A main impact of the source remediation event was a DOC release from the soil and aquifer material, which stimulated microbial activity and reduced the redox conditions in the aquifer, such that a zone 1050 to 1400 m from the source was suitable for reductive dechlorination of cDCE and VC. It was determined from the first and second major sampling campaigns that PCE and TCE underwent biotic degradation in the first 400 m of the plume before remediation and in the first 1000 m of the plume after remediation. It was also determined that cDCE did not undergo degradation in the first 1050 m from the source zone, before the remediation event, but 8 years later did undergo biotic degradation within 1000 m from the source zone. Degradation of cDCE and VC in the plume was documented; it was not possible to ascertain the exact mechanism of cDCE (and VC) degradation from 1400 m until the plume front, but in both 2006 and 2014, there is evidence that a combination of reductive dechlorination and abiotic degradation was responsible.

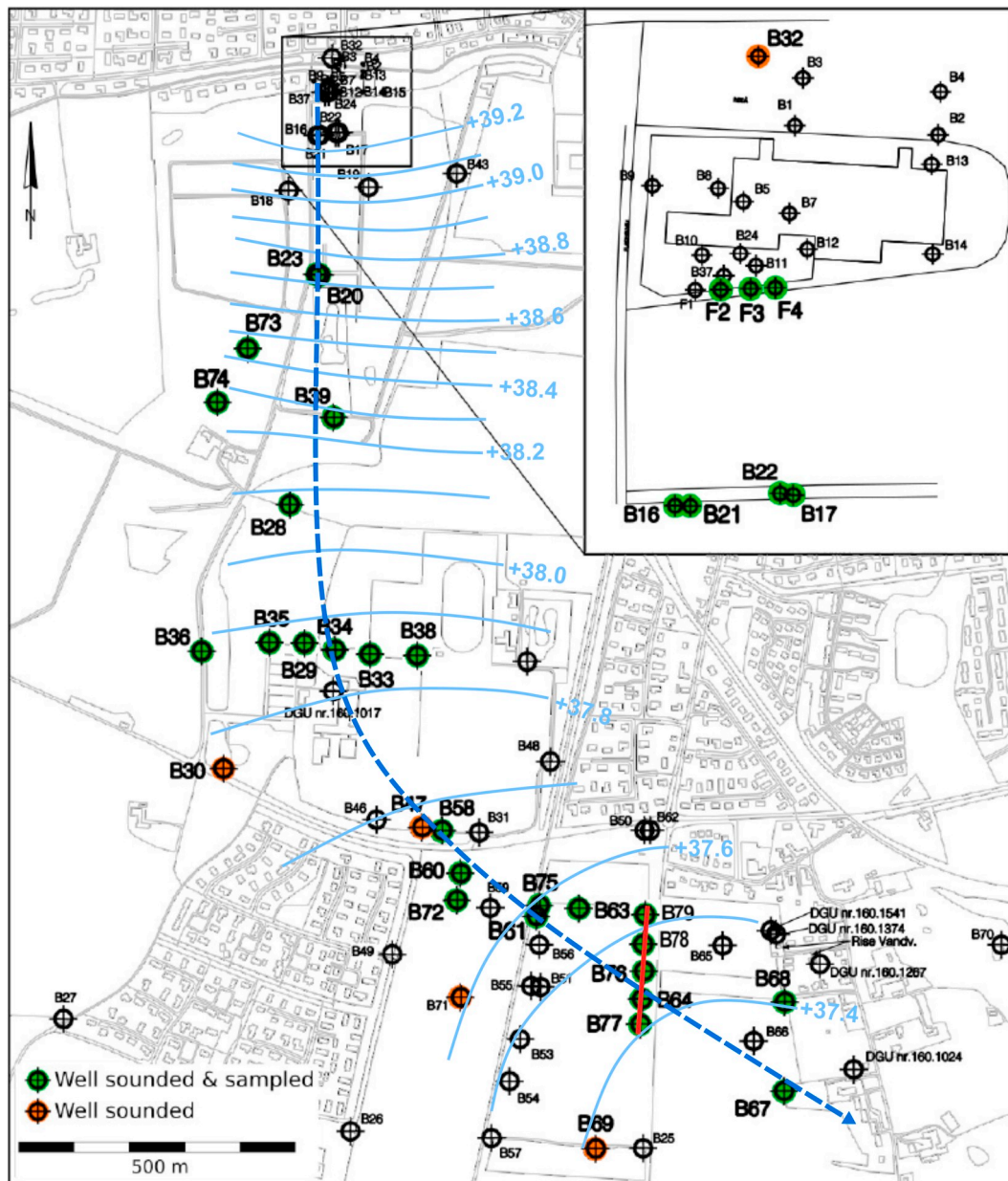


Fig. 1. Sampling scheme for the 2017 sampling campaign, groundwater equipotential lines from 2017 (light blue), and approximate plume flowline (dashed dark blue). All well locations indicated with a colour (both green and orange) were sounded; well locations indicated in green were also sampled. Map insert shows the source zone and sampled wells (F2, F3, and F4) that are immediately downgradient from the source. Detailed information about which analyses were conducted at each sampled location is included in Table S1. (For interpretation of the references to colour in this figure legend, the reader is referred to the web version of this article.)

Since 2014, five new wells have been drilled, these are B75, B76, B77, B78, and B79 (Fig. 1). Wells B76 through B79 are located directly north and south of well B64 and form a 100 m transect across the plume near the front, at 1900 m from the source. Wells B36, B35, B29, B34, B33, and B38 form another transect across the plume at 1050 m from the source. The flow line of the plume was determined based on measurements taken in these transects, and it was determined that the flowline was the same as in the previous two studies. More information on the new transect can be found in the Supplementary Information.

3. Materials and methods

3.1. Hydraulic testing: slug tests and pump tests

Vacuum slug tests were conducted in duplicate on 25 screens in six

boreholes (Table S2) during the 2017 field investigation. Pump tests were also conducted on nine of these screens in three boreholes. Data was collected using Slug Test Acquisition® software (Geoprobe Systems®) and analyzed with AQTESOLV Pro® software (HydroSOLVE, Inc.); the Springer-Gelhar and Kansas Geological Survey models were used to interpret the slug test data and determine the hydraulic conductivity for the sandy, underdamped and clayey, overdamped portions of the Rødrekro aquifer, respectively. Pump test data were analyzed with the Theis solution (Theis, 1935).

3.2. Groundwater sampling

In the 2017 sampling campaign, which spanned 4 weeks in March–April, 52 screens from 24 boreholes were sampled (Fig. 1, Table S1). Boreholes not on the flowline that formed the two transects were

sampled at a later date (Fig. 1, Table S1). Sampled boreholes are indicated in green in Fig. 1. An additional nine boreholes were sounded during the campaign, indicated in orange in Fig. 1. Sampling procedures were the same as those used in the previous two campaigns (Badin et al., 2016; Hunkeler et al., 2011) except for the following minor differences. Sampling materials for nitrate (NO_3^-), sulfate (SO_4^{2-}), ferrous iron (Fe(II)), manganese (Mn^{2+}), and methane (CH_4) were provided by Eurofins (Eurofins Miljø A/S, Denmark). Samples for chlorinated ethene isotope analysis were acidified with HCl; 40 mL samples were collected in quadruplicate, and 1 L samples were collected in duplicate. Samples for analysis by Microbial Insights were taken with Sterivex™ filters and fastenings provided by Microbial Insights, Inc. (Knoxville, TN, USA) and were stored in 50 mL Falcon tubes at -10°C until shipment to Microbial Insights (Microbial Insights Europe, Wondelgem, Belgium) for analysis. Samples for 16S rRNA amplicon sequencing and *rdhA* analysis were collected by passing 0.93–3 L of groundwater through a 0.22 μm Sterivex™ filter (Millipore Corporation Billerica, MA, USA) via vacuum pump and were flash frozen in the field in liquid N_2 . Samples were stored at -80°C before analysis at Aarhus University (AU) in Roskilde, Denmark or shipment on dry ice to Ecole Polytechnique Fédérale de Lausanne (EPFL) in Switzerland. Samples for rRNA analysis were collected by passing 4–5 L of groundwater through a 0.2 μm MicroFunnel™ filter (Pall Corporation, Port Washington, NY, USA) via vacuum pump, stored in a Cryo-Tube (Nunc A/S, Roskilde, Denmark), and were flash frozen in the field in liquid N_2 and stored at -80°C before analysis at AU in Roskilde, Denmark.

3.3. Analyses

3.3.1. Chemical analysis

All sampled well screens were analyzed for aqueous redox relevant chemical parameters as well as for PCE and its degradation products. Of these, 37 well screens were also analyzed for the gases methane, ethene, ethane, and acetylene (Fig. 1, Table S1). Analyses for aqueous NO_3^- , Mn^{2+} , Fe(II), SO_4^{2-} , and DOC were conducted by the accredited (DANAK, ISO/IEC 17025) laboratory Eurofins in Veen, Denmark (Package AAG, Eurofins Miljø A/S, Denmark) with detection limits of 0.3 mg L^{-1} , 0.005 mg L^{-1} , 0.01 mg L^{-1} , 0.5 mg L^{-1} , and 0.1 mg L^{-1} respectively. PCE, TCE, cDCE, and VC were also analyzed by Eurofins with a gas chromatography-mass spectrometer (GC-MS) and a detection limit of $0.02\text{ }\mu\text{g L}^{-1}$ for all compounds. Methane, ethene, ethane, and acetylene were measured at the Technical University of Denmark (DTU, Kongens Lyngby, Denmark) using a headspace gas chromatograph with a flame ionization detector (GC-FID) (Thermo Scientific TRACE 1300 GC with HP-plot Q capillary column $8\text{ m} \times 0.32\text{ mm/I.D. } 0.02\text{ mm}$, Agilent Technologies). The detection limit was $0.05\text{ }\mu\text{g L}^{-1}$ for methane and $0.25\text{ }\mu\text{g L}^{-1}$ for ethene, ethane, and acetylene and the results were processed with Chromeleon software (Thermo Scientific).

3.3.2. Isotopic analysis

Samples from 37 well screens (Table S1) were collected for compound specific isotope analysis (CSIA) for carbon and chlorine. Carbon isotope ratios ($^{13}\text{C}/^{12}\text{C}$) were measured with an isotope ratio mass spectrometer coupled to a gas chromatograph by a combustion interface (GC-C-IRMS) at the University of Neuchâtel (CHYN, Switzerland) using the method described by (Badin et al., 2016) with detection limits of $30\text{ }\mu\text{g L}^{-1}$, $30\text{ }\mu\text{g L}^{-1}$, $25\text{ }\mu\text{g L}^{-1}$, and $7\text{ }\mu\text{g L}^{-1}$ for PCE, TCE, cDCE, and VC, respectively. Sets of Vienna Pee Dee Belemnite (VPDB) referenced standards of PCE, TCE, and cDCE were prepared and analyzed in the same manner as the samples to correct for isotope fractionation which may occur during sample preparation and analysis. A purge and trap system was applied, with a purge volume of 25 mL. For samples with chlorinated ethene concentrations lower than these detection limits, a purge volume of 1 L was applied (Badin et al., 2016), and detection limits for carbon isotope fractionation were $1.3\text{ }\mu\text{g L}^{-1}$,

$1.1\text{ }\mu\text{g L}^{-1}$, $0.8\text{ }\mu\text{g L}^{-1}$, $0.6\text{ }\mu\text{g L}^{-1}$ for PCE, TCE, cDCE, and VC, respectively. Chlorine isotope ratios ($^{37}\text{Cl}/^{35}\text{Cl}$) were also measured as previously described by Badin et al. (2016) for PCE and TCE, with minimum required concentrations for analysis of $30\text{ }\mu\text{g L}^{-1}$ and $5\text{ }\mu\text{g L}^{-1}$, respectively. Chlorine isotope ratios were obtained by measuring pairs of ion fragments using a quadrupole mass spectrometer following separation with a gas chromatograph. During each measuring sequence the samples were bracketed with two external standards referenced to the Standard Mean Ocean Chloride (SMOC) in order to allow reporting of sample isotope ratios relative to SMOC using a two-point calibration.

3.3.3. Molecular biology analysis

Six samples from wells along the centerline of the plume (F3, F4, B23, B34, B58, B61) and one sample from the outer fringe of the plume (B75-1) were sent to Microbial Insights (Microbial Insights Europe, Wondelgem, Belgium) for QuantArray®-Chlor analysis, which includes quantitative polymerase chain reaction (qPCR) for multiple organohalide-respiring genera (*Dehalococcoides*, *Dehalobacter*, *Dehalogenimonas*, *Desulfitobacterium*, *Dehalobium*, and *Desulfuromonas*) and *rdhA* genes (*tceA*, *bvcA*, *vcrA*, and the newly identified *cerA*, capable of degrading VC to ethene (Yang et al., 2017)).

DNA and rRNA extraction was conducted at AU for all other microbial samples. Sterivex™ filters were opened up, and both the Sterivex™ and MicroFunnel™ filters were pulverized. DNA was then extracted, purified, and in some cases up-concentrated from the Sterivex™ filters and rRNA from the MicroFunnel™ filters. Analyses for the specific degrader genera *Dehalococcoides* and *Dehalogenimonas* were conducted via qPCR. Primer and thermocycling information is included in the SI. Because there is only one 16S rRNA gene per *Dehalococcoides* genome, qPCR results of copies L^{-1} are equivalent to cells L^{-1} (Ritalahti et al., 2006). Sufficient genetic material was obtained from wells F2, F4, B16, B17, and B23 (Table S1) for specific degrader and gene qPCR analysis. Sufficient rRNA for activity analysis was collected from wells F4, B17, and B23 (Bead-Beat Total RNA kit, A&A Biotechnology, Polen). Remaining DNA was removed (DNase I, RNase-free, Thermo Fisher Scientific, US) and cDNA was produced using a High-Capacity cDNA Reverse Transcription kit with RNase Inhibitor (Thermo Fisher Scientific, US). The cDNA was analyzed by qPCR for content of *Dehalococcoides*, *bvcA*, and *vcrA* (Bælum et al., 2013).

Eleven of the DNA samples extracted from the Sterivex™ filters were sent to EPFL for community analysis via 16S rRNA amplicon sequencing (F2, F4, B16, B17, B23, B34, B58, B61, and B64). DNA samples were amplified by PCR with adapter-containing primers LBE-AS-27F and LBE-AS-338R with Q5 High-Fidelity polymerase (BioLabs) (see SI for primer and thermocycling information). PCR products were first purified with Agencourt AMPure XP beads according to the manufacturer's instructions and quantified with the Fragment Analyser (DNF-473 standard sensitivity NGS fragment analysis kit, Advanced Analytical Technologies Inc., U.S.A). Addition of 12-nt barcodes, final sample preparation, and sequencing in paired-end mode (2x250bp) were performed by the Genomic Technologies Facility (GTF, University of Lausanne, Switzerland) following the standard Illumina MiSeq protocol (Illumina, Inc., CA, USA). Analysis of the raw amplicon sequences was performed using a custom python bioinformatics pipeline developed at the Laboratory for Environmental Biotechnology at EPFL. First, the sequences were de-multiplexed and the barcodes were removed. Sequences were then trimmed with Timmomatic-0.36 and contigs formed with PEAR version 0.9.11 (Zhang et al., 2014). Clusters were created using CD-HIT-EST with 97% identity and $n = 5$ and aligned using Infernal 1.1.2 (Nawrocki and Eddy, 2013) in order to remove non-16S rRNA sequences. The aligned clusters were blasted against the Greengenes database (McDonald et al., 2012) to attribute operational taxonomic units (OTUs) to the entire cluster using similarity thresholds of 75.0% for phylum, 78.5% for class, 82.0% for order, 86.5% for family, and 94.5% for genus (Yarza et al., 2014). OTUs were categorized

by functional group as described in [Badin et al. \(2016\)](#); the category assignments are included in Table S5 in the Supplementary Information.

3.4. Calculations

3.4.1. Pore water velocity and contaminant transport

The pore water velocity was calculated for the locations where slug and pump tests were performed using the Darcy equation (Eq. (1)), and the distance a particle would move downgradient without degradation or dispersion was calculated using Eq. (2):

$$v_{p,i} = \frac{K_i \cdot I}{\varphi} \quad (1)$$

$$d_i = \frac{v_{p,i} \cdot t}{R} \quad (2)$$

where $v_{p,i}$ [m d^{-1}] is the pore water velocity at location i ; K_i [m d^{-1}] is the hydraulic conductivity at location i ; I [-] is the hydraulic gradient; φ [-] is the porosity; d_i [m] is the distance the aqueous species moves downgradient in a given time, t [d], given a starting location in the aquifer, i ; and R [-] is the retardation factor, a ratio of the pore water velocity to the velocity of the aqueous species ([Nazaroff and Alvarez-Cohen, 2001](#)). K_i was determined as described in [Section 3.1](#). I was calculated from the hydraulic potential map. Typical values for a Danish aquifer were selected for φ , 0.35 for sand and 0.5 for clay ([Appelo and Postma, 2005](#)). The distance an aqueous species would move downgradient was calculated piecewise, where the aquifer was divided into three discrete flow zones, i , based on the location of clay lenses in the geology. These zones were from 0 to 700 m from the source, 700–1200 m from the source, and > 1200 m from the source. Each flow zone was attributed an average K_i based on the slug test results. When calculating transport of the chlorinated ethene contamination, a value of 1.2 was selected for R for PCE and TCE based on values determined empirically from chlorinated ethene transport in sand aquifers with low organic content ([Kret et al., 2015](#)). Because the octanol-water partition coefficient for cDCE is nearly half that of PCE ([Cwiertny and Scherer, 2010](#)), R for cDCE was assumed to be 1.

3.4.2. Isotope balance, extent of degradation, and degradation rates

Carbon isotope results are presented as a fraction of $^{13}\text{C}/^{12}\text{C}$ relative to the VPDB international standard in delta notation, where $\delta = (R/R_{\text{std}} - 1) \cdot 1000$ [‰] and R and R_{std} are the ratio of the heavy isotope to the light isotope in the sample and the standard, respectively ([Hunkeler et al., 2011](#)). Chloride isotopes are presented in the same manner as the ratio of $^{37}\text{Cl}/^{35}\text{Cl}$ relative to the SMOC international standard. In order to determine whether degradation to compounds which were not detected occurred to a significant degree, the $\delta^{13}\text{C}$ balance was calculated as in [Badin et al. \(2016\)](#).

The extent of degradation and the degradation rates were calculated based on the $\delta^{13}\text{C}$ values relative to the initial relative carbon isotope

fraction, $\delta^{13}\text{C}_0$, of the mother compound PCE, which was determined in ([Hunkeler et al., 2011](#)) to be -25 ‰. When all of the mother compound has been converted to a daughter compound, that daughter compound can be treated as the mother compound for calculation of the degradation rate. The extent of degradation (D) as a fraction was calculated using Eq. (3) ([Badin et al., 2016](#)):

$$D = 1 - \exp\left(\frac{\Delta\delta^{13}\text{C}}{\varepsilon}\right) \quad (3)$$

Where ε [‰] is the enrichment factor. An enrichment factor for carbon, ε_C , of -8.4 ‰ was found by using dual C-Cl plots ([Section 4.4.1](#)) and was applied to estimate the degradation extent of PCE. Literature values were applied for cDCE; due to uncertainty of the dominating degradation pathway, minimum and maximum enrichment values were found from literature ranges for both biotic and abiotic pathways. For biotic reductive dechlorination of cDCE, the ε_C range is -14.1 ‰ to -31.1 ‰ ([Bloom et al., 2000](#); [Lihl et al., 2019](#)). For abiotic dechlorination of cDCE, the ε_C range is -6.9 ‰ to -21.7 ‰ ([Elsner et al., 2008](#); [Vanstone et al., 2004](#)). The enrichment factors applied for estimating the extent of cDCE degradation were thus -6.9 ‰ and -31.1 ‰.

First order degradation rates for ^{12}C were calculated using Eq. (4), modified from ([Morrill et al., 2005](#)) to include the retardation factor, R :

$$k_{CE,i}^{12} = \frac{-\left(\frac{1000}{\varepsilon}\right) \cdot \ln\left(\frac{\delta^{13}\text{C}/1000 + 1}{\delta^{13}\text{C}_0/1000 + 1}\right)}{R \cdot L / v_{p,i}} \quad (4)$$

where $k_{CE,i}^{12}$ [d^{-1}] is the first order degradation rate for ^{12}C in chlorinated ethene CE in location i , and L [m] is the distance from the location where degradation began. For PCE this is the source, and for cDCE this is where $\delta^{13}\text{C}_{\text{cDCE}} = \delta^{13}\text{C}_{0,\text{PCE}}$. A degradation rate can also be calculated based on location rather than distance by replacing the denominator in Eq. (4) with time between the measurements. Half-lives, $T_{1/2}$, were calculated by $\ln(2)/k_{CE,i}^{12}$.

4. Results and discussion

4.1. Hydraulic conductivity and pore water velocity

The hydraulic conductivity determined by the slug and pump tests generally agreed, though the hydraulic conductivity measured by the pump tests was consistently one order of magnitude lower than that measured by the slug tests. The hydraulic conductivity was determined to be $1.97 \times 10^{-3} \text{ m s}^{-1}$ (170 m d^{-1}) on average in the underdamped portions of the aquifer and $2.11 \times 10^{-4} \text{ m s}^{-1}$ (18 m d^{-1}) in the overdamped portions. Hydraulic conductivity data for both the slug and pump tests is included Table S2 and Fig. S2 in the Supplementary Information.

The pore water velocity along the central flow line decreases with distance from the source zone ([Fig. 2](#)). For the first 400 m downgradient from the source, a clay lens at 20 meters below ground surface (mbgs)

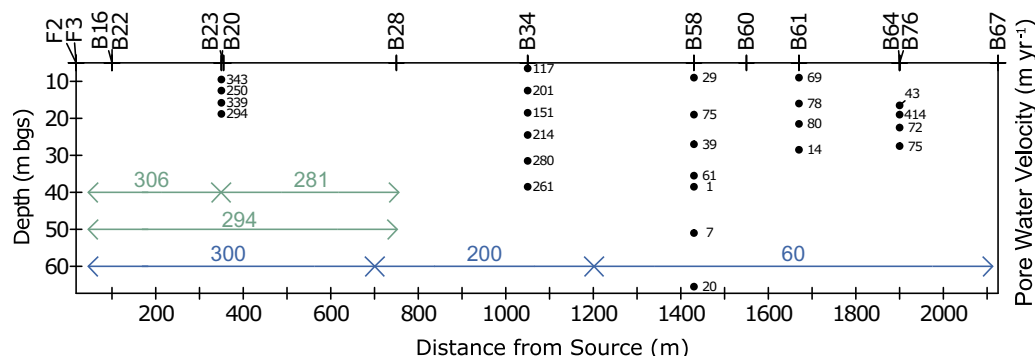


Fig. 2. Pore water velocity along the approximate plume flowline, calculated using hydraulic conductivity values determined via slug tests conducted in 2017. The arrows represent assumed pore water velocities for specific distances to assess transport (blue) and for estimation of degradation rates (green). (For interpretation of the references to colour in this figure legend, the reader is referred to the web version of this article.)

constricts the groundwater flow; when the lens is no longer present, the pore water velocity slows down. By 1400 m from the source, the pore water velocity is approximately ten times less than the velocity 400 m from the source, with local variations likely due to a few significant clay lenses present in this portion of the aquifer. The pore water velocity from the source zone to 700 m is approximately 300 m yr^{-1} on average. In the transitional section from 700 to 1200 m from the source zone, where the plume is no longer confined by the clay lens at 20 mbgs and expands in the vertical direction, the average pore water velocity is 200 m yr^{-1} . From 1200 m to the plume front, the average pore water velocity is approximately 60 m yr^{-1} . Representative, rather than average, pore water velocity values were chosen for each section.

In 2006, the hydraulic conductivity of the aquifer, based on one pump test, was estimated to be $6.5 \times 10^{-4} \text{ m s}^{-1}$, corresponding to a groundwater velocity of 0.24 m d^{-1} or 87 m yr^{-1} with parameters typical for a sandy, Danish aquifer. It was estimated that from 2006 to 2014, chlorinated ethenes could be expected to be transported 600 m downgradient without degradation. Using local pore water velocities determined in 2014 and 2017 without degradation is as follows: PCE and TCE near the source zone would be transported approximately 750 m downgradient; cDCE near the longitudinal center of the plume, near B34, would be transported approximately 600 m downgradient; and cDCE in the last portion of the plume, near wells B58 to B64, would be transported approximately 150 m downgradient.

4.2. Redox conditions

The redox conditions in and along the length of the plume are variable, and adds interest to the continued investigation of the plume. Interpreted redox profiles for all three sampling campaigns are depicted in Fig. 3. Measured concentrations of individual redox sensitive species

for the 2006 and 2014 sampling campaigns have been published previously (Badin et al., 2016; Hunkeler et al., 2011), and 2017 redox data for individual parameters are included in Fig. S3 in the Supplementary Information.

From 2014 to 2017, little change was documented in the O_2 and NO_3^- reducing zones. The maximum O_2 concentration is 6.12 mg L^{-1} in 2017, compared to 6.40 mg L^{-1} in 2014 (Badin et al., 2016). In 2010, O_2 measurements were below detection in the previously oxic part of the plume, presumably due to the DOC release (Badin et al., 2016). In 2017, O_2 and NO_3^- concentrations are above 1 mg L^{-1} at depths above 10–15 mbgs and above 20 mbgs, respectively. While concentrations of O_2 and NO_3^- are $< 0.1 \text{ mg L}^{-1}$ below these depths, Fe(II) and SO_4^{2-} appeared at concentrations of $0.36\text{--}0.45 \text{ mg L}^{-1}$ and $43\text{--}61 \text{ mg L}^{-1}$, respectively, indicating the location of the pyrite oxidation front at approximately 20 mbgs as described in the previous site investigations (Badin et al., 2016; Hunkeler et al., 2011).

Mixed redox conditions are still present near the source zone at the local scale, as was also documented in 2014, but not in 2006. As in 2014, O_2 and Fe(II) are sometimes measured simultaneously in some screens within 20 mbgs and 100 m from the source (especially F2, F3 and F4). There are also some screens in this area where NO_3^- and Fe(II) are not detected, but methane is detected in low concentrations ($< 0.01 \text{ mg L}^{-1}$). The DOC released by the thermal remediation (Friis et al., 2005) is still measured at its highest concentration, 6.9 mg L^{-1} , in the mixed area, and is similar to the 6.1 mg L^{-1} measured in 2014. Mn (II) was not measured in 2014, but in 2017 was measured at low levels of $0.28\text{--}0.51 \text{ mg L}^{-1}$ throughout the aquifer and appeared in its highest concentration, 3.9 mg L^{-1} , in the mixed zone. In Badin et al. (2016), it was posited that this mixed zone was the result of local subsurface heterogeneity impacted at different rates by the DOC released by the thermal remediation. Anoxic pockets in mixed redox zones can provide ideal conditions for reductive dechlorination (Wiegert et al., 2012) and

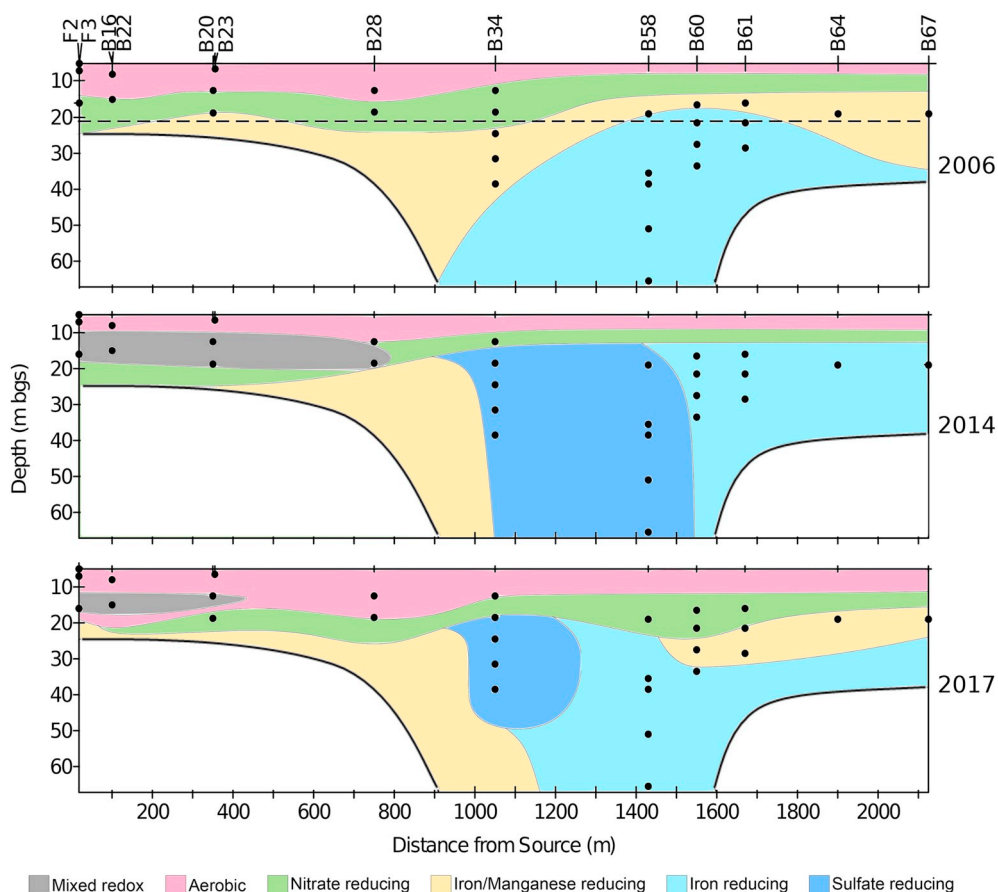


Fig. 3. Interpreted redox zonation for each major sampling campaign. Information used to create the 2006 interpretation is from the sampling campaign carried out in both 2006 and 2007. The dotted line in the 2006 interpretation indicates the approximate location of the pyrite oxidation front. Blank areas, without redox zonation, in each bottom corner of the figure represent areas with no data, where it is assumed that the original iron/manganese reducing condition of the aquifer remains. (For interpretation of the references to colour in this figure legend, the reader is referred to the web version of this article.)

it is possible that this process occurs in this zone. Though the mixed zone has decreased in size, this effect of the thermal remediation is still present in 2017.

Just as the most marked change from 2006 to 2014 was the appearance of an SO_4^{2-} reducing zone, the most marked change from 2014 to 2017 is that the SO_4^{2-} reducing zone has become smaller. In 2014, Fe(II) was not detected from 1050 to 1400 m from the source zone. In 2017, Fe(II) is present throughout the aquifer at depths > 20 mbgs. Fe(II) concentrations at 1050 m downgradient in 2017 are 0.25–0.37 mg L^{-1} , which is less than its presence in the remainder of the aquifer, at 0.47–1.2 mg L^{-1} . SO_4^{2-} concentrations in the aquifer at depths > 20 mbgs range from 36 to 50 mg L^{-1} as in the two previous sampling campaigns, where the lowest concentrations are concurrent with the lowest Fe(II) concentrations, in well B34. This indicates that SO_4^{2-} reduction still occurs in this zone, but to a lesser extent than before – there is no longer enough biogenic sulfide, the product of SO_4^{2-} reduction, to form iron-sulfide precipitates with all Fe(II) produced by pyrite oxidation. However, there is still a decrease in the SO_4^{2-} concentration, which indicates that iron-sulfide precipitates, also referred to as reactive mineral intermediates, are still present at this location (Culpepper et al., 2018; Jeong et al., 2011).

The decrease in size of the SO_4^{2-} reducing zone and the increased concentration of O_2 since 2010 indicate that the redox conditions of the aquifer are returning to their state prior to the thermal remediation and influx of DOC in 2006. However, the conditions in the aquifer are still favorable for microbial respiration of cDCE and VC (Scheutz et al., 2010) in the mixed zone near the source and in the SO_4^{2-} reducing section of the plume, between 1000 and 1200 m from the source.

4.3. Evolution of chlorinated ethene concentrations

The concentrations of PCE and its daughter compounds, TCE, cDCE, and VC, were measured in the plume as in previous sampling campaigns (Badin et al., 2016; Hunkeler et al., 2011) and data for 2017 are presented in Fig. 4a. Ethene, ethane, and acetylene were also measured, but as in previous campaigns, were not detected. The plume in general still follows the previously measured centerline.

PCE and TCE are still detected in the first 1050 m and 1400 m from the source, respectively, as in 2014, but the concentrations are generally lower than in 2014 and remain substantially lower than before the thermal remediation was conducted. The PCE and TCE centers of mass appear to have moved downgradient since 2014, although the maximum concentrations are found in the same boreholes. PCE still dominates the first 750 m of the plume by mole fraction (Fig. 4b), especially at depths > 10 mbgs, but unlike in 2014, PCE mole fractions over 85% only occur near the source zone. TCE concentrations within 350 m from the source have also decreased from 2014 to 2017, although the highest concentrations in B28, B34, and B58 have remained relatively constant.

cDCE remains the dominating chlorinated ethene in the plume, and the highest cDCE concentrations are still found in B34, 1050 m from the source, where the plume enters the more reducing zones of the aquifer. In the first 750 m of the plume, the mole fraction of cDCE has decreased since 2014, though it is still the dominating chlorinated ethene in the mixed zone at < 10 mbgs within 350 m from the source. Concentrations measured near and at the plume front remain similar to those measured in 2014 and remain higher than what was measured before the remediation event in 2006.

VC is mostly detected from 1050 m from the source until the front of the plume, and VC concentrations are generally lower than in 2014 and 2006. The highest VC concentration was found in well B34, as was also the case in 2006 and 2014. The VC mole fraction at the plume front has decreased from 40% in 2014 to 16% in 2017. While the maximum concentrations of cDCE and VC in well B34 have moved further downgradient than in 2014, indicating that the plume is moving in the longitudinal direction, there is no indication that the contaminants

have moved the 150 to 500 m estimated from the local pore water velocity calculations, which suggests that degradation is occurring.

4.4. Carbon and chlorine isotope composition and evolution

The carbon and chlorine isotope values were measured as in the two previous sampling campaigns (Badin et al., 2016; Hunkeler et al., 2011); the 2017 data is presented in Table S3, and the distribution of carbon isotope values are shown on Fig. 4b. The $\delta^{13}\text{C}$ values have not changed remarkably since 2014. The $\delta^{13}\text{C}$ values for PCE are more enriched than the initial value, previously estimated to be -25% (Hunkeler et al., 2011), in all but one sampling point. This documents PCE degradation within the first 750 m from the source. The $\delta^{13}\text{C}$ signatures for TCE in this part of the plume indicate that TCE is produced and then even further degraded in some parts above the pyrite oxidation front at approximately 20 mbgs. The most noteworthy degradation of TCE occurs as the plume crosses the pyrite oxidation front at B34, 1050 m downgradient from the source, with $\delta^{13}\text{C}$ values of $+11\%$ and $+7.2\%$.

In the mixed redox zone, the first 350 m of the plume, the $\delta^{13}\text{C}$ values for cDCE indicate production followed by degradation, reaching a $\delta^{13}\text{C}$ value of up to -20.4% . Within 350–750 m downgradient from the source, cDCE production is primarily observed, with the lowest $\delta^{13}\text{C}$ values of -33.6% and -37.1% . As the plume enters the sulfate reducing zone at B34, 1050 m downgradient from the source, cDCE degradation occurs, with $\delta^{13}\text{C}$ values from -20.6% to -23.9% , with the exception of the deepest screen at ~ 40 mbgs where there is no documentation for degradation. From 1430 m to the plume front, there is also no documentation for cDCE degradation, as the $\delta^{13}\text{C}$ values are close to the initial signature, with the exception of B76 at a distance of 1900m, where the $\delta^{13}\text{C}$ is enriched to -22.4% . However, a small amount of cDCE degradation could still occur but not be documented if production is the dominant process.

Immediately downgradient from the source zone, a $\delta^{13}\text{C}$ value for VC of -18.1% suggests degradation, whereas values of -26.5% to -36.7% indicate VC production at 100–1050 m. From 1050 m to the plume front, the VC concentrations were too low for isotope analysis; isotope signatures can therefore not be used to assess if the produced VC is further degraded in this part of the plume. As with cDCE, the trend in B76 is an exception in the last part of the plume, where the $\delta^{13}\text{C}$ for VC is enriched and thus indicates further degradation.

Since the contamination originates from one source, an isotopic mass balance can be applied to assess if all degradation products were accounted for (Aeppli et al., 2010; Blazquez-Pali et al., 2019) and was determined for all points with available isotope data (Table S3). Enriched $\delta^{13}\text{C}_{\text{sum}}$ values are found within the first 100 m, at 1050 m (B34), and at 1900 m (B76) from the source. These areas correspond to where cDCE degradation is documented by the $\delta^{13}\text{C}$ values. VC is detected at these locations, and though isotope signatures are not available at all locations to document further dechlorination, it is possible that this enrichment could be due to further degradation of VC. This would indicate that degradation of cDCE is the rate limiting step in the dechlorination process. However, the enrichment could also be an effect of cDCE degradation by a different process without significant VC production, e.g. abiotic degradation by iron minerals below the pyrite oxidation front (Lee and Batchelor, 2002a). End-products of anaerobic reductive dechlorination (ethene and ethane) and of abiotic degradation by e.g. pyrite (acetylene, ethene, and ethane) were not detected and could not be used for clarification. The remaining points have a $\delta^{13}\text{C}_{\text{sum}}$ value close to the initial value, indicating that all contaminants are accounted for and that a limited reduction of the total contaminant mass occurs at 350 m and again from 1450 m to the front of the plume.

The isotope time series data also provide information about areas of the plume between sampling points. As an example, the enrichment in $\delta^{13}\text{C}$ signatures for cDCE observed at 1050 m in 2014 still occurs in 2017, but the enriched signatures are not observed in the downgradient

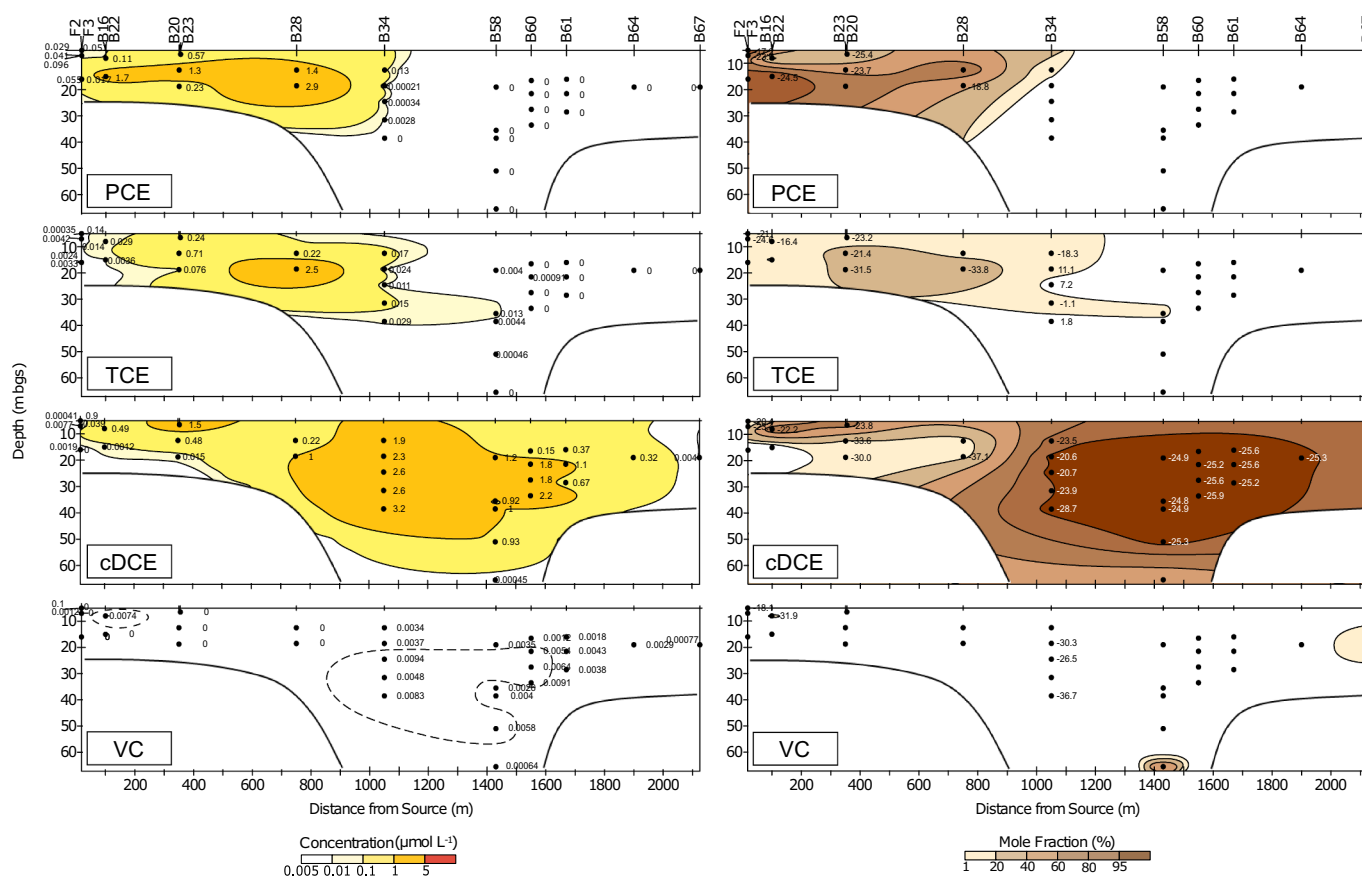


Fig. 4. Chlorinated ethene concentrations (a) and mole fraction contours (b) in the subsurface from the 2017 sampling campaign. Data point labels indicate concentration measurements in (a) and $\delta^{13}\text{C}$ measurements in (b), also from the 2017 sampling campaign. Blank areas, without contour information, in each bottom corner of the figure are areas with no data. (For interpretation of the references to colour in this figure legend, the reader is referred to the web version of this article.)

monitoring wells at 1430 m. Given the average pore water velocities (Section 4.1), the transport time between these locations is approximately 4–5 years. Because the less enriched values documented in the sulfate reducing zone in 2014 are not measured at 1430 m from the source in 2017, the zone where cDCE was degraded in 2014 must have been < 200 m in length. The data also indicate that the degradation zone was not present in 2010, as again, less enriched cDCE isotope signatures would have been detected downgradient in the 2017 sampling campaign. This corresponds well with redox parameters measured in 2010, as Fe(II) was present and the sulfate reducing zone was only beginning to form at well B34, and supports the process understanding of the plume evolution.

4.4.1. Dual C-Cl isotope plots

Dual-isotope plots for all monitored years (2006 (Hunkeler et al., 2011), 2014 (Badin et al., 2016), and 2017) are presented in Fig. 5, to provide insight into degradation pathways and changes over time. For the dual-isotope assessment, these slopes are compared to other reported slopes related to different pathways for the individual compounds (Table 1).

The dual C-Cl slope for PCE of 2.2 found in 2017 corresponds well with the slope of 3.0 obtained in 2014. These values are within the range of the reported slopes for microbial reductive dechlorination (0.7 to 3.8), which is one of the most well documented degradation pathways for chlorinated ethenes by the dual C-Cl isotope technique (Table 1). This supports that PCE is degraded by biotic reductive dechlorination within the first 750 m of the plume, however slopes that correspond to other pathways have yet to be defined for PCE. Nonetheless, the likelihood that this pathway occurs is also supported by the high concentration of the intermediate product TCE.

At the current knowledge level, the reported slopes (Table 1) are not a strong indicator to determine the degradation pathway for TCE at the field site. First, because recent investigation of slopes related to TCE oxidation (-38 to 1.7) covers a great span, as the investigated strains, *Pseudomonas putida* F1 and *Methylosinus trichosporium* OB3b, produce degradation related slopes that are both steeper and more gradual than the slopes of the other pathways. Gafni et al., 2018 does state that further research is required to resolve uncertainties about whether the OB3b strain that led to the 1.7 slope is representative of this pathway. If this result is excluded from the range corresponding to TCE oxidation (-38 to ∞), the slopes related to this pathway can be separated from the others. Secondly, Lihl et al., 2019 recently found that cultures precultivated on DCE and VC provided steeper slopes (9.0–18.2) for TCE dechlorination than the commonly reported range (2.3–4.8). Thus, biotic and abiotic slopes for TCE degradation overlap, as the only reported slope for abiotic TCE reduction (5.2) is within the range of biotic reductive dechlorination (2.3–18.2). The dual C-Cl slopes for TCE of 2.4 and 2.7 found at this study site, in 2017 and 2014, respectively, are lower than the reported slope for abiotic degradation, which could indicate that TCE degradation in the first 1050 m of the plume is primarily due to biotic reductive dechlorination. This is supported by the significant production of cDCE throughout the plume. However, additional investigation is required to strengthen the applicability of the dual C-Cl isotope approach to assess TCE degradation pathways.

For cDCE, it was not possible to obtain $\delta^{37}\text{Cl}$ results in 2017, and it is therefore not possible to evaluate if the observed change in slope from 1.8 to 3.0 in 2006 to 2014 remains. In 2014, it was assessed that cDCE degradation was predominantly abiotic (3.1 to 5.0), as the slopes did not match reported values for microbial reductive dechlorination (11.4–13.7) at the time (Table 1). The same conclusion can be drawn

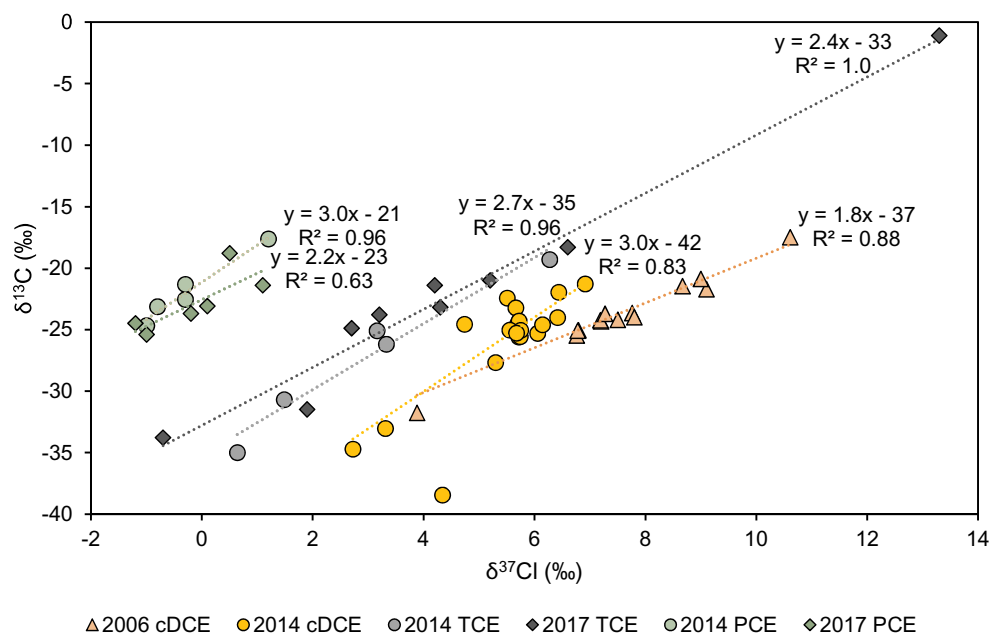


Fig. 5. Dual C-Cl isotope slopes for PCE, TCE, and cDCE degradation. Results are included from the current sampling campaign as well as the two previous sampling campaigns in 2006 (Hunkeler et al., 2011) and 2014 (Badin et al., 2016). (For interpretation of the references to colour in this figure legend, the reader is referred to the web version of this article.)

including new slopes reported in the literature: abiotic (3.1 to 5.0), chemical oxidation (-125), microbial oxidation (32.3), and microbial reductive dechlorination (4.5 to 17.8) (Table 1). It is notable that the slope range for microbial reductive dechlorination is now closer to the slopes found in the Røddekro site investigations. The slopes found at Røddekro are also comparable to a slope recently reported for combined biotic reductive dechlorination and abiotic dechlorination (1.5) (Table 1). The possibility that both degradation pathways occur in the plume for cDCE should therefore not be dismissed. This is elaborated upon in combination with other lines of evidence in Section 5.

Dual C-Cl isotope slopes can provide site specific enrichment factors (ϵ_C). The parallel trend between the PCE and TCE slopes confirms that PCE is the precursor to TCE. The offset of the intercepts on the $\delta^{13}C$ axis can thus be used to determine the ϵ_C for this degradation step (Hunkeler et al., 2009). This results in an enrichment factor of -8.4‰ in 2017; for comparison it was estimated to be -10.3‰ based on the 2014 dataset. It is viable to apply dual isotope analysis to estimate the enrichment factor at the field scale, as this estimation method is not dependent on concentration and therefore not impacted by dispersion and transport processes. Further, the data used for the ϵ_C estimation is not the same as that used for estimation of the extent of degradation and degradation rates. These site-specific enrichment factors are within the range of earlier reported values of -3.6‰ (Badin et al., 2014), -5.6‰ (Wiegert et al., 2013) and -19.0‰ (Cretnik et al., 2014).

4.4.2. Quantification of degradation by isotope fractionation

The extent of degradation was calculated by Eq. (3) for PCE in the first 750 m of the plume and for cDCE from 1050 m to the plume front (Table S3), as this estimation can only be done for compounds that solely are degraded (Badin et al., 2016). This approach has been applied successfully at several field sites (e.g. Aeppli et al., 2010; Lollar et al., 2001) and uncertainties related to this estimation method have been assessed to be relatively low (Abe and Hunkeler, 2006; Thullner et al., 2012).

The extent of PCE and cDCE degradation are comparable between 2014 and 2017, as would be expected since the $\delta^{13}C$ values are similar in both sampling campaigns. The main development is that the extent of PCE degraded at B28-1 (750 m downgradient) has increased from 30% to 52%. The largest proportion of degraded PCE is estimated to be 61% in F3-3 (18 m downgradient), while the average extent of PCE degradation is 29% in the first 750 m of the plume. This demonstrates

that degradation varies spatially, and that a significant proportion of PCE must be degraded between 750 m and 1050 m downgradient from the source. The estimation of degraded cDCE is more uncertain, since a site-specific enrichment factor related to cDCE degradation could not be obtained. The largest proportion of degraded cDCE is estimated to lie between 13% and 47% and is found in B34-4, 1050 m downgradient from the source zone. In B58, 1430 m downgradient, at most 2% of cDCE is estimated to be degraded, which illustrates that cDCE is chiefly degraded in the sulfate reducing zone.

The isotope data can also be applied to derive degradation rates, and though there is some uncertainty related to the input parameters, it is still suggested to be a more accurate approach than determining rates from concentrations (Abe and Hunkeler, 2006; Morrill et al., 2005). Local degradation rates were calculated for PCE (Table 2) by dividing the plume into two flow zones from 18 to 350 m and from 350 to 750 m downgradient from the source (see Supplementary Information for more information on flow assumptions). The apparent degradation rate for the first 350 m (0.12 yr^{-1}) is three times lower than the rate for 350 m to 750 m (0.35 yr^{-1}). The estimated degradation rate (0.25 yr^{-1}) for the entire length (0–750 m) demonstrates that averaging over a longer distance masks the local variation, and it is thus important to determine local pore water velocities if the isotope signatures indicate local degradation zones. The degradation rates between the same boreholes and screens were also estimated using data from previous sampling campaigns, under the assumption that flow conditions were the same. The estimated degradation rate for the first 350 m of the plume compares well between 2006 (0.17 yr^{-1}), 2014 (0.14 yr^{-1}) and 2017 (0.12 yr^{-1}), though the degradation rate appears to become slower over time. There is a more remarkable change from 350 m to 750 m, as the estimated rate is approximately 3 times larger in 2017 (0.35 yr^{-1}) compared to 2014 (0.11 yr^{-1}), though similar to the rate from 2006 (0.41 yr^{-1}). The difference is caused by a weaker enrichment of PCE in B28-1 (750 m downgradient) in 2014, contrary to what would have been expected from the development in redox conditions. The data reveal that degradation quantification estimations are sensitive to redox conditions not only in the longitudinal direction but also in the vertical direction; as an example another screen measured in 2014, B23-2, would have provided a degradation rate of 0.53 yr^{-1} between the source and 350 m downgradient (compared to the 0.14 yr^{-1} above). It is therefore important to combine this assessment with other lines of evidence to understand at which spatial orientation

Table 1

Dual C-Cl isotope slopes compared with values from the literature for PCE, TCE, and cDCE degradation at the field and laboratory scales. Some slopes have been converted to ensure the same ratio and allow for comparison between all data, the original reported slopes are included in parentheses.

Degradation process	Compound	Scale	Dual isotope slope (ϵ_C/ϵ_{Cl})	Reference
Abiotic	TCE	Laboratory	5.2 ± 0.3	Audí-Miró et al. (2013)
	cDCE	Laboratory	3.1 ± 0.2	Audí-Miró et al. (2013)
		Laboratory	5.0 ± 0.6	Audí-Miró et al. (2013)
Biotic anaerobic reductive dechlorination	PCE	Field	0.9	Wiegert et al. (2012) ($\epsilon_{Cl}/\epsilon_C = 1.12$)
		Field	2.4	Wiegert et al. (2012) ($\epsilon_{Cl}/\epsilon_C = 0.42$)
		Field	0.7 ± 0.3	Badin et al. (2014)
		Field	3.5 ± 1.6	Badin et al. (2014)
		Field	2.2	This study (2017)
		Field	3.0	This study (2014)
		Laboratory	2.9	Wiegert et al. (2013) ($\epsilon_{Cl}/\epsilon_C = 0.35$)
		Laboratory	2.7 ± 0.3	Badin et al. (2014)
		Laboratory	0.7 ± 0.2	Badin et al. (2014)
		Laboratory	3.8 ± 0.2	Cretnik et al. (2014)
	TCE	Field	2.4	This study (2017)
		Field	2.7	This study (2014)
		Laboratory	2.7	Wiegert et al. (2013) ($\epsilon_{Cl}/\epsilon_C = 0.37$)
		Laboratory	3.4 ± 0.2^a	Cretnik et al. (2013)
		Laboratory	3.4 ± 0.2^a	Cretnik et al. (2013)
		Laboratory	3.8 ± 0.2	Cretnik et al. (2013)
		Laboratory	4.8	Kuder et al. (2013) ($\epsilon_{Cl}/\epsilon_C = 0.21$)
		Laboratory	3.2 ± 0.2	Buchner et al. (2015)
		Laboratory	3.4 ± 0.2	Buchner et al. (2015)
		Laboratory	2.8 ± 0.3	Buchner et al. (2015)
		Laboratory	3.5 ± 0.2	Buchner et al. (2015)
		Laboratory	3.1 ± 0.1	Lihl et al. (2019)
		Laboratory	2.7 ± 0.2	Lihl et al. (2019)
		Laboratory	2.3 ± 0.1	Lihl et al. (2019)
		Laboratory	11.8 ± 2.4	Lihl et al. (2019)
		Laboratory	18.2 ± 4.3	Lihl et al. (2019)
		Laboratory	9.0 ± 1.1	Lihl et al. (2019)
		Laboratory	4.5 ± 0.8	Lihl et al. (2019)
	cDCE	Laboratory	13.7	Abe et al. (2009) ($\epsilon_{Cl}/\epsilon_C = 0.073$)
		Laboratory	11.4	Abe et al. (2009) ($\epsilon_{Cl}/\epsilon_C = 0.088$)
		Laboratory	4.5 ± 3.4	Doğan-Subaşı et al. (2017)
		Laboratory	10.0 ± 0.4	Lihl et al. (2019)
Laboratory		17.8 ± 1.0	Lihl et al. (2019)	
Combined biotic and abiotic	cDCE	Field	1.5 ± 0.15^b	Audí-Miró et al. (2015)
		Field	3.0	This study (2014)
		Field	1.8	This study (2006)
Oxidation	TCE	Laboratory	1.7 ± 0.4^c	Gafni et al. (2018)
		Laboratory	-38 ± 27^c	Gafni et al. (2018)
		Laboratory	∞^d	Doğan-Subaşı et al. (2017)
	cDCE	Laboratory	32.3^c	Abe et al. (2009) ($\epsilon_{Cl}/\epsilon_C = 0.031$)
		Laboratory	-125 ± 47^d	Doğan-Subaşı et al. (2017)

^a This value was found twice in the study but for two different microbial strains: *G. lovleyi* SZ and *D. hafniense* Y51.

^b Combined biotic anaerobic reductive dechlorination and abiotic degradation by iron minerals, but with the former dominating.

^c Microbial aerobic oxidation.

^d Oxidation by permanganate.

it is most reasonable to assume similar conditions and thus which estimated degradation rates are most representative for a given stretch of the plume. Regardless, neither estimated rate is large enough to completely degrade PCE within the first 750 m. Although there is some variation in the estimated degradation rates, they are in general at the low end of the literature reported range of $0.3\text{--}7.3\text{ yr}^{-1}$ (Ottosen et al., 2019). Thus, PCE degradation likely continues between 750 m and 1050 m downgradient from the source, as the plume crosses the pyrite oxidation front and enters the sulfate-reducing zone. Indeed, the PCE concentration drops so low between these locations (Fig. 4) that isotope analysis was not possible at 1050 m downgradient from the source.

The degradation observed for cDCE was so localized that degradation rates over distance could not be estimated from the 2017 data.

However, because degradation occurred in the same area in 2014 and 2017, a degradation rate can be calculated through time rather than space. The rate was estimated for two depths at 1050 m downgradient from the source where there was enrichment over time, which revealed maximum degradation rates of 0.03 yr^{-1} and 0.07 yr^{-1} . These degradation rates are low compared to the literature reported range of $0.3\text{--}3.3\text{ yr}^{-1}$ (Ottosen et al., 2019). The results highlight the importance of determining site-specific enrichment factors, as the literature reported ϵ_C range resulted in at least a three-fold difference in the estimated degradation rates.

A time-based degradation rate was also estimated for PCE in B28-1, where the change of degradation extent was greatest between 2014 and 2017. Interestingly, the degradation rate found at this one location, at

Table 2

Estimated degradation rates for PCE and cDCE as a function of distance and time, where L = distance for calculation, t = time frame for calculation, V_p = pore water velocity at calculation location (more information in SI), k = degradation rate, and $t_{1/2}$ = contaminant half-life.

	Part of plume	ϵ_c (‰)	$\delta^{13}C_0$ (‰)	$\delta^{13}C$ (‰)	L (m)	t (yr)	V_p (m yr ⁻¹)	k (yr ⁻¹)	$t_{1/2}$ (yr)
PCE 2017	0–350 m	–8.4	–25	–23.7	350	–	306	0.12	5.8
	350–750 m		–23.7	–18.8	400	–	281	0.35	2.0
	0–750 m		–25	–18.8	750	–	294	0.25	2.8
PCE 2014	0–350 m	–10.3	–25	–23.1	350	–	306	0.14	5.0
	350–750 m		–23.1	–21.3	400	–	281	0.11	6.3
	0–750 m		–25	–21.3	750	–	294	0.12	5.8
PCE 2006	0–350 m	–10.3	–25	–22.6	350	–	306	0.17	4.1
	350–750 m		–22.6	–15.5	400	–	281	0.41	1.7
	0–750 m		–25	–15.5	750	–	294	0.31	2.2
cDCE 2014–2017	1050 m (B34-3)	–6.9 & –31.1	–21.3	–20.7	–	3	–	0.03–0.01	23–69
	1050 m (B34-4)	–	–22	–20.6	–	3	–	0.07–0.02	10–35
PCE 2014–2017	750 m (B28-1)	–8.4 & –10.3	–21.2	–18.8	–	3	–	0.10–0.08	6.9–8.7

750 m, (0.08 yr⁻¹ or 0.10 yr⁻¹, depending on the applied enrichment factor) is equivalent to the one found between immediately down-gradient from the source and 750 m (0.12 yr⁻¹). The travel time from the source to 750 m downgradient is approximately 3 years, the same period as is evaluated in the time-based degradation rate; the estimated rate in one location over time corresponds to what occurred over the upgradient distance in the same time frame.

4.5. Specific degrader quantification and bacterial community composition

In order to further understand the extent to which chlorinated ethene biodegradation processes occur in the plume, 16S rRNA gene amplicon sequencing and specific gene/degrader qPCR analyses were conducted for the genera *Dehalococcoides* and *Dehalogenimonas*. Activity transcription analysis based on RNA was also conducted for *Dehalococcoides*, *bvcA* and *vcrA*. It is not uncommon for RNA extraction to be unsuccessful for subsurface samples (Richards et al., 2019), and RNA was only quantifiable in three samples. However, in these three screens where RNA was quantifiable, the qPCR signal was indistinguishable from the acceptable negative control, which indicates either no activity or that insufficient biomass was collected in the sample.

Both *Dehalococcoides* and *Dehalogenimonas* were detected throughout the plume, with the highest concentrations of 1.4×10^5 cells L⁻¹ and 3.7×10^6 cells L⁻¹, respectively, found just down gradient of the source zone (Table 3). These abundances are comparable to those found in similar naturally degrading plumes (Damgaard et al., 2013). It is prudent to note, however, that microbial abundance measurements from groundwater samples have limitations. Groundwater

samples allow collection of only those microorganisms that are not sorbed to the porous media (Griebler et al., 2009) and may not accurately represent what is present in the subsurface. Additionally, microbial community composition and the abundance of specific degraders in the subsurface varies greatly at the centimeter scale, as was determined with high resolution sampling in Damgaard et al., 2013 and Richards et al., 2019. Discrete sediment sampling in a deep, saturated sandy aquifer, as is found at Rødekro, is not feasible. The abundances presented in Table 3 represent a large sample collection area, and relatively few samples were collected along a plume length of 2 km. While there are limitations that may prevent, for example, rate quantification based on microbial populations, microbial abundance measurements from groundwater samples do reflect OHRB distribution throughout the plume, and knowledge of which OHRB are present along the contaminant plume is requisite for process understanding.

In well B34-3, in the sulfate reducing zone where conditions are favorable for biotic degradation of cDCE and VC, both *Dehalococcoides* and *Dehalogenimonas* were present, however *Dehalococcoides* was not at all detected in B58-6, the first well after the sulfate reducing zone. *Dehalogenimonas* was present in higher amounts than *Dehalococcoides* in all measured locations except in B75-1, 1680 m from the source zone, where both concentrations were lowest; both concentrations here were three and four orders of magnitude lower than the highest concentrations nearest the source zone. Auxiliary analyses conducted at Aarhus University show that both specific degrader genera were also detected at B16-1 and B17-1, approximately 100 m from the source zone (Table S4). Prior to recognition of the *Dehalogenimonas* capability to use cDCE and VC as electron acceptors (Yang et al., 2017), those wells with no

Table 3

Quantitative organohalide respiration relevant genera and functional gene data, as analyzed by Microbial Insights; bd = below detection, where the detection limit is 1.00×10^2 cell L⁻¹ or copies L⁻¹ for all analyses except *cerA*, where detection limits are indicated in the table.

Well-screen	F3-3	F4-3	B23-1	B34-3	B58-6	B61-1	B75-1
Distance from source (m)	18	18	350	1050	1430	1670	1670
Depth (m bgs)	5	5	19	24.5	19	28.5	26.5
<i>Dehalococcoides</i> spp. (cells L ⁻¹)	1.40×10^5	1.10×10^5	5.00×10^2	4.10×10^3	bd	5.00×10^2	4.00×10^2
<i>vcrA</i> (copies L ⁻¹)	4.80×10^3	1.70×10^3	1.00×10^{2a}	bd	bd	bd	bd
<i>bvcA</i> (copies L ⁻¹)	3.40×10^4	2.10×10^4	bd	2.30×10^3	bd	bd	bd
<i>Dehalogenimonas</i> spp. (cells L ⁻¹)	2.80×10^6	3.70×10^6	9.00×10^4	4.90×10^4	2.90×10^3	6.10×10^3	3.00×10^{2b}
<i>cerA</i> (copies L ⁻¹)	1.80×10^{3c}	2.00×10^{3d}	bd ^e	bd ^e	bd ^e	bd ^f	bd ^g
<i>Dehalobacter</i> spp. (cells L ⁻¹)	1.96×10^6	7.55×10^5	3.32×10^4	4.36×10^5	4.52×10^5	6.93×10^5	1.22×10^6
<i>Desulfotobacterium</i> spp. (cells L ⁻¹)	1.55×10^6	1.74×10^6	4.10×10^4	2.21×10^4	4.66×10^4	1.68×10^4	8.40×10^4
<i>Desulfuromonas</i> spp. (cells L ⁻¹)	1.23×10^7	3.99×10^7	1.44×10^6	9.81×10^4	3.80×10^6	1.89×10^5	5.88×10^6

^a Result is below reporting limit of 3.00×10^2 copies L⁻¹ but above detection limit.

^b Result is below reporting limit of 3.50×10^3 copies L⁻¹ but above detection limit.

^c Result less than reporting limit of 2.50×10^3 copies L⁻¹ and greater than detection limit of 5.00×10^1 copies L⁻¹.

^d Result less than reporting limit of 3.30×10^3 copies L⁻¹ and greater than detection limit of 6.70×10^1 copies L⁻¹.

^e Detection limit of 5.00×10^1 copies L⁻¹.

^f Detection limit of 5.10×10^1 copies L⁻¹.

^g Detection limit of 6.90×10^1 copies L⁻¹.

measured *Dehalococcoides* population would not be identified as exhibiting the potential for complete dechlorination. In other studies, *Dehalogenimonas* may be present in locations where *Dehalococcoides* was not detected but lower chlorinated ethenes were detected (Badin et al., 2016; Nijenhuis et al., 2007). The presence of these known degraders, especially at higher concentrations immediately downgradient from the source zone, indicates the possibility that the microbial community is capable of complete biotic reduction of PCE to ethene.

The genera *Dehalobacter*, *Desulfitobacterium*, and *Desulfuromonas*, which contain species that are capable of partial PCE dechlorination, were detected at relatively high concentrations throughout the plume. *Dehalobacter* was detected in the pyrotag sequencing analysis in 2014, but the Microbial Insights QuantArray analysis is the first documentation of presence of *Desulfitobacterium* and *Desulfuromonas* in the Rødekro plume.

Dehalococcoides VC reductase genes *vcrA* and *bvcA* were detected within 1050 m from the source zone (Table 3), where $\delta^{13}\text{C}$ indicate cDCE degradation. Auxiliary analyses at Aarhus University detected *vcrA* at wells within 100 m from the source (Table S4). The *cerA* gene from *Dehalogenimonas*, which codes for the enzyme responsible for reductive dechlorination of vinyl chloride to ethene (Yang et al., 2017), was only detected in F3-3 and F4-3, directly downgradient from the source zone. Expression of the genes to respire VC is a positive indication of the occurrence of this process in this portion of the plume (Liang et al., 2017); non-detection of the genes does not indicate the reverse, as other currently unidentified genes or bacteria may be capable of carrying out this respiration process.

16S rRNA gene amplicon sequencing yielded information as to the relative abundance of the entire microbial community in each sampled screen. Operational taxonomic units (OTUs) known to represent anoxic redox and degradation functional guilds were included in the analyses, including Organohalide Respiring-Respiring Bacteria (OHRB), Organohalide Cometabolic/Oxidizing Bacteria (OHCB), Sulfate Reducing Bacteria (SRB), Iron Reducing Bacteria (FeRB), and Iron Oxidizing Bacteria (FeOB) (Table S5). OHRB were further divided into the categories partial and total, where OHRB-partial denotes those OTUs with known capability to dechlorinate PCE and TCE to cDCE and OHRB-total denotes those OTUs with known capability to dechlorinate cDCE and VC to ethene. Guilds that were not selected for in depth analysis accounted for approximately three quarters of the reads in each sample and include, for example, fermenting and aerobic bacteria.

Fig. 6 shows that the OHRB total and partial guilds combined

account for up to 14% of the total reads in some samples. This portion is consistently greater than that of other guilds, such as SRB, and indicates that organohalide respiration is a significant enough process to support a substantial portion of the total microbial community. Most OHRB OTUs are those with partial degradation capability; the exception to this is screen B17-1, 100 m from the source zone, where 44% of the selected OTUs represent bacteria with the capacity to degrade cDCE and VC, with the primary contribution from the genus *Dehalogenimonas*. However, B17-1 was not analyzed for *cerA*, so it is not possible to ascertain whether these *Dehalogenimonas* express this VC *rdhA* gene. The largest OTUs identified to partially respire chlorinated ethenes are those in the Dehalococcoidales order and Dehalococcoidaceae family that could not be further classified to a family or genus. It is therefore possible that some of these reads could belong to the *Dehalococcoides* or *Dehalogenimonas* genera, which were coded as OHRB-total, but were unable to be identified as such.

The OHRB guilds are present throughout the plume, and their relative abundances generally decrease with increased distance from the source, which corroborates the trend seen in the specific degrader DNA analyses. These results match well with pyrotag sequencing data from 2014, where *Dehalococcoides* and *Dehalogenimonas* were found throughout the plume, and also with specific degrader analyses conducted by GEUS in 2014, where *Dehalococcoides* was detected, but were below the quantification limit throughout the portion of the plume that is 1050 m and further from the source (i.e. the sulfate reducing zone and the plume front). It could be that these bacteria were present and active in this area in 2014, but were first definitely quantifiable in 2017 due to the time it may take for the bacteria to establish themselves. *Dehalobacter*, *Desulfitobacterium*, and *Desulfuromonas*, detected in the Microbial Insights analysis in 2017, were not found in the 2017 community sequencing analysis. Imfeld et al. (2010) also found that more OHRB genera were detectable using taxon specific rather than clone library analysis. In the 2017 sequencing analysis, the only reads assigned to the Peptococcaceae family, which includes both *Dehalobacter* and *Desulfitobacterium*, belonged to the SRB *Desulfosporosinus meridiei* (Robertson et al. (2001)), though *Dehalobacter* was detected in the pyrotag sequencing in 2014 using the same sequence library, Green-genes.

OHCB were detected consistently throughout the plume, though at low relative abundance as compared to the OHRB. Aerobic oxidation of chlorinated ethenes has been documented to occur in what are typically labelled anaerobic conditions that contain as little as 0.1 mg L^{-1} of

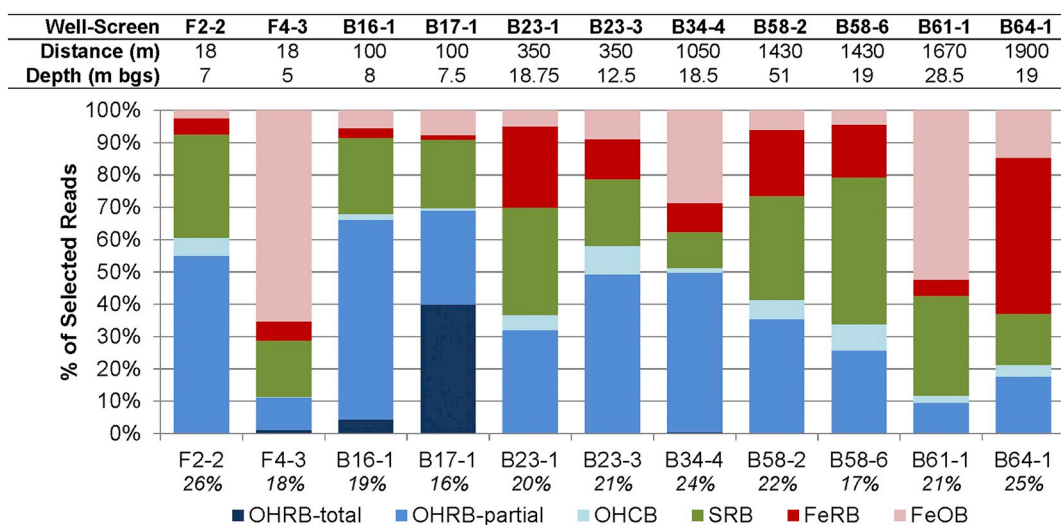


Fig. 6. 16S rRNA gene amplicon sequencing results, where the bar plot shows the distribution of the relative abundance of selected reads and the italicized percentage below each column denotes the proportion of the selection to the total number reads in each sample. Distance indicates distance from the source zone. (For interpretation of the references to colour in this figure legend, the reader is referred to the web version of this article.)

dissolved oxygen (Gossett, 2010; Richards et al., 2019). However, all measured concentrations of oxygen below the pyrite oxidation front were an order of magnitude lower than this limit (see Supplementary Information). Additionally, the genes *etnE* and *etnC* were not detected by the Microbial Insights QuantArray analysis at any point in the plume, which suggests etheneotrophs implicated in cometabolic aerobic degradation of VC are not active (Liang et al., 2017).

Possible SRB, FeRB, and FeOB containing OTUs are observed in all measured wells. The relative proportion of FeRB in each well has increased to 2%–48% in 2017, as compared to 0%–4% in 2014, which is consistent with the redox chemical parameters that show less reduced conditions in 2017 as compared to 2014. B64-1 in particular, at 1900 m from the source zone, exhibits a large relative abundance of FeRB and low relative abundance of OHRB. The low abundance of OHRB is consistent with the lower concentrations of chlorinated ethenes at the plume front, and the higher relative abundance of FeRB is consistent with indications from the redox chemical analyses. Multiple factor analyses at chlorinated ethene contaminated sites have shown that VC reduction and iron reduction are competing processes (Shani et al., 2013), and thus the capability for the microbial community to reduce iron at this section of the plume may inhibit VC reduction. However, it should be noted that FeRB and FeOB are phylogenetically diverse, which renders their identification in the Illumina sequencing results more uncertain than for the specialists OHRB and OHCB (Weber et al., 2006). Pyrite oxidation is in general carried out by FeOB (Schippers and Jorgensen, 2002; Silverman, 1967). While F4-3, which is closest to the surface, and B61-1, which is located at 28.5 mbgs, both have larger selected proportions of FeOB, these bacteria also appear to be more or less well distributed throughout the length and depth of the plume. OTUs purportedly capable of sulfate reduction were identified in all wells; there was no distinct trend at B34-4, in the sulfate reducing zone. Some SRB are facultative and can use electron acceptors other than sulfate, which could explain their ubiquitous distribution in the plume (Castro et al., 2000). Sulfate reduction has been shown to inhibit organohalide respiration (Berggren et al., 2013; Murray et al., 2019), but has also in some cases stimulated dechlorination (Harkness et al., 2012; Murray, 2019). The two processes, sulfate reduction and DCE dechlorination, have been documented to occur concurrently by geochemical and microbial community analysis in a constructed wetland, which is similar to the Rødøkro plume in that it is an anoxic, sandy environment (Imfeld et al., 2010). Microbial community interactions are complex; metabolic complementarity in the microbial community and the functional capabilities of the organisms that support OHRB may play an important role in stimulation or inhibition of dechlorination (Hug et al., 2012; Murray, 2019; Pérez-De-Mora et al., 2014; Wang et al., 2019).

The microbial analyses in general show that there is the possibility for anaerobic reductive, aerobic metabolic, or co-metabolic degradation of chlorinated ethenes throughout the plume, including at 1050 m from the source in the sulfate reducing zone. The capability for complete reduction is strongest directly downgradient of the source zone, where the genes *vcrA*, *bvcA*, and *cerA* are detected, and weakest at the plume front, where FeRB are present in the highest relative abundance.

5. Degradation mechanisms/summary

The information provided by the physical, chemical, isotopic, and microbial lines of evidence can be combined to create one comprehensive, holistic picture of the fate and transport of chlorinated ethenes (Badin et al., 2016; Courbet et al., 2011; Hunkeler et al., 2011; Nijenhuis et al., 2018, 2007), as was done in the Rødøkro plume. The overview of the degradation mechanisms cannot only be elucidated spatially, but also temporally when the results from all three sampling campaigns are analyzed collectively, as depicted in Fig. 7. Fig. 7-2017 includes all new information from the current study. Fig. 7-2006 and Fig. 7-2014 are re-depictions of data presented in Hunkeler et al. (2011)

and Badin et al. (2016), respectively. The colored boxes in Fig. 7 coarsely delineate various areas of the plume with common characteristics.

The effect of the source zone thermal remediation on the plume is the most marked change between 2006 and 2014. In 2006, chlorinated ethene concentrations were very high immediately downgradient from the source zone depicted in Fig. 7 as the black box. After the remediation, this area became reduced due to the released DOC, biotic degradation began to take place, and the chlorinated ethene concentrations decreased by 85%. Biotic degradation was also enhanced in the red and orange boxes, and *Dehalococcoides* was present and active here in 2014, unlike before the remediation event. The DOC release also reduced conditions further from the source, and a sulfate reducing zone, depicted in blue, was identified in 2014. Isotopic signatures provided evidence that decreases in TCE and cDCE concentrations were indeed due to degradation. Conditions in this reduced zone were favorable for biotic degradation, though *Dehalococcoides* was only present, and at low abundance and activity, at one point between well B34 and the plume front in 2014. This is similar to results from 2006, where a *Dehalococcoides* signal, below the quantification limit, was observed in two screens between well B34 and the plume front.

The enhanced degradation continued to be apparent in 2017, and the evolution of the plume can be determined using the multiple lines of evidence. Despite that active *Dehalococcoides* populations were not detected in 2017, the microbial line of evidence overall more firmly indicates biotic degradation than in previous sampling campaigns as the specific degraders *Dehalococcoides* and *Dehalogenimonas* and VC *rdhA* genes were detected throughout the plume in 2017, with the exception that no VC *rdhA* genes were detected near the plume front. This is a marked change from 2014, where *Dehalococcoides* was principally located within the first 350 m from the source, and no VC *rdhA* genes were detected. Another overall change is that the $\delta^{13}\text{C}$ values for cDCE have become more enriched in some key locations, though isotopic evidence of degradation is found in the same locations in 2017 as in 2014.

In the area immediately downgradient from the source, indicated by the red boxes, all chlorinated ethenes were detected in both 2014 and 2017. The $\delta^{13}\text{C}$ were enriched for all chlorinated ethenes in 2017 and indicate that TCE and cDCE are degradation products, rather than impurities, as was the case in 2006. The local anoxic areas suitable for anaerobic cDCE reduction in the mixed redox zone were still present in 2017. Unlike in 2014, however, all three analyzed VC *rdhA* genes were detected. The isotopic evidence combined with expression of these genes by *Dehalococcoides* and *Dehalogenimonas* is a strong indication that VC is biotically degraded in this area.

The mixed zone extends past the red boxes in both 2014 and 2017, though it has decreased in size, and dual C-Cl isotope slopes indicate that when PCE and TCE are degraded in the red, orange, and green boxes, the mechanism is anaerobic reductive dechlorination. Thus, biotic degradation still occurs here as in 2014; however, the $\delta^{13}\text{C}$ values for TCE show that TCE is no longer degraded in the deeper part of the plume at 350 m downgradient from the source, represented by the change in shape of the green box. The rate at which PCE is degraded between the orange and the green box is three times higher than in 2014, yet in both years, PCE is fully converted to daughter compounds before reaching the blue box. VC was detected in neither the orange nor the green boxes in both years. In 2017, *vcrA* was detected, which indicates that VC is used an electron acceptor and degradation past cDCE may occur in this area. Community sequencing data in 2017 also show that bacteria that may be capable of complete dechlorination comprise 44% of the community in B17-1, in the orange box.

The sulfate reducing zone, depicted as the blue box, is still present in 2017, though it is less reduced than in 2014 and has decreased in size. The redox conditions appear to slowly be returning to the conditions prior to the remediation event, though the impact after one decade is still strong and apparent; the presence of *Dehalococcoides*,

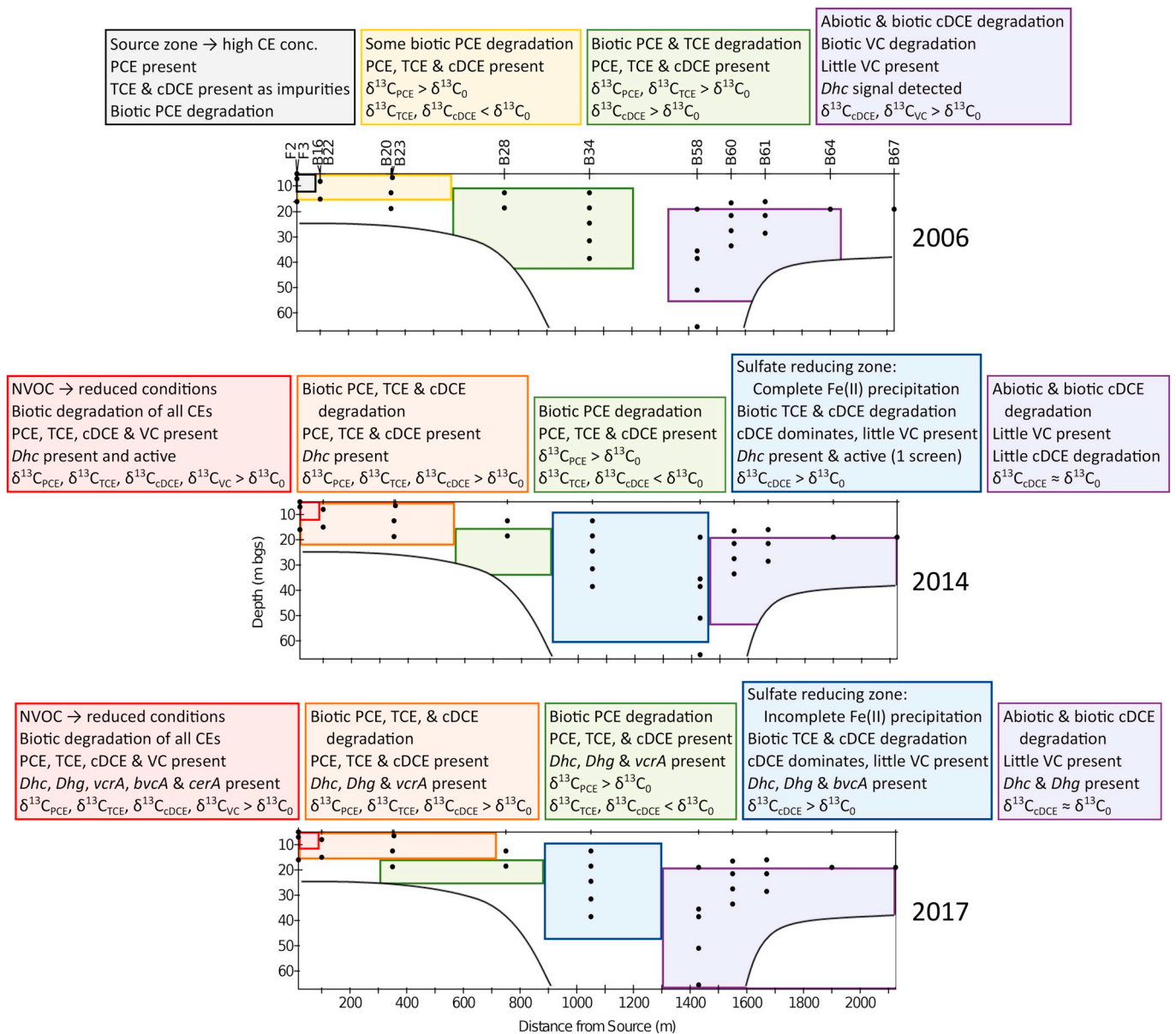


Fig. 7. Summary of conditions and degradation mechanisms present in the plume during each major sampling campaign. The colored boxes coarsely delineate zones in the plume where different conditions/processes occur and the relevant parameters found in these zones. Parameters not discussed in the boxes indicate both not measured and not detected. CE = chlorinated ethene, *Dhc* = *Dehalococcoides* spp., *Dhg* = *Dehalogenimonas* spp. (For interpretation of the references to colour in this figure legend, the reader is referred to the web version of this article.)

Dehalogenimonas, and *bvcA* indicate that biotic degradation occurs in this area. The enriched $\delta^{13}C$ values for cDCE document that it is degraded here, however because Cl isotopic ratios for cDCE could not be obtained in 2017, dual isotope plots are not available to assess the degradation pathway. Dual isotope plots from the previous sampling campaigns suggest the mechanism could be anaerobic reductive dechlorination and/or abiotic degradation by iron minerals. The shortest estimated half-lives for cDCE in this area of the plume are 23 and 10 years for 2014 and 2017, respectively, and the conditions favorable for anaerobic reductive dechlorination would need to be present for at least a kilometer to reduce the concentration of cDCE to half of its 2014 level. The slow rate is insufficient to completely reduce cDCE within the blue box, which is disappearing, though this may be compensated for by increased degradation prior to the chlorinated ethenes entering this reduced zone. The evolution of this dynamic can be investigated in future sampling campaigns.

The plume front is more or less stationary; from 2014 to 2017, it has

moved downgradient significantly less than would be expected from groundwater transport. While it may be that the clay lens that begins 1500 m from the source influences the contaminant transport, the stationary nature of the plume is most likely evidence that the cDCE that enters the purple box undergoes a destructive process. VC concentrations in the purple box in 2017 are low, such that measurement of the isotopic signature was not possible. However, in 2006 both cDCE and VC $\delta^{13}C$ values were enriched in this part of the plume, documenting that transformation of both compounds occurred. The low concentrations of VC measured in 2017 may be due to abiotic degradation of cDCE, where VC is not produced or is produced in small amounts (Lee and Batchelor, 2002a), or may be because biotic cDCE degradation is the rate limiting step. Though well B76 was deemed to be on the plume fringe rather than on the flowline (see SI), the VC $\delta^{13}C$ ratio in well B76 shows significant enrichment, which is evidence that VC degradation occurs at this location. This point may only provide insight to the local conditions at well B76, or may be representative of this area of the

plume, where VC concentrations are too low to measure isotopic signals. cDCE isotopic analyses along the plume centerline do not document that degradation of cDCE occurs in this area of the plume, as the $\delta^{13}\text{C}$ values for cDCE were nearly the same as the $\delta^{13}\text{C}_0$. It is possible that cDCE here is degraded via a mechanism/bacterial strain that does not influence the $\delta^{13}\text{C}$ ratios, though it is expected that during future sampling campaigns, the enriched cDCE detected at well B34 in 2014 would be detected in well B58 the purple box. *Dehalococcoides* and *Dehalogenimonas* were detected in the purple box, though no VC reductase genes were detected. Non-detection of the VC reductase genes does not necessarily indicate that VC reduction does not occur, as lower chlorinated ethene concentrations in total would provide fewer electron acceptors for this bacterial guild, and thus these bacteria would be present in smaller quantities and are possibly below detection. It is also possible that VC respiration in this part of the plume is facilitated by currently unidentified species or genes or by microaerophilic or anaerobic oxidation (Bradley et al., 1998; Liang et al., 2017; Smits et al., 2011).

Chlorinated ethenes can be degraded abiotically by pyrite to become acetylene (Lee and Batchelor, 2002a). Although abiotic reduction by iron sulfide minerals is well documented in laboratory experiments, the degradation products are easily converted to readily biodegradable compounds, so it is difficult to document in situ (Liang et al., 2009). Additionally, it is not well investigated, especially in comparison to biotic degradation (He et al., 2015). The stable iron sulfide mineral pyrite is commonly found in sandy Danish aquifers, but it is also likely that other iron sulfide minerals are present, such as mackinawite or amorphous FeS precipitate as a result of sulfate reduction. Both cDCE and VC have been shown to be reactive with a number of iron minerals, such as pyrite and green rust (Lee and Batchelor, 2002a, 2002b), however there are conflicting results on whether cDCE degradation can be mediated by mackinawite (Hyun and Hayes, 2015; Jeong et al., 2011). While it is possible that abiotic reduction of chlorinated ethenes does occur in the aquifer based on the presence of iron-sulfide minerals and dual C-Cl isotope slopes, it is not possible to establish that any particular mechanism is responsible. Information provided by the different lines of evidence are not necessarily mutually exclusive – the detection of specific degraders does not exclude the possibility that abiotic degradation also occurs. From 1450 m downgradient from the source to the plume front, chlorinated ethenes do undergo a destructive process, and it is likely that some combination of abiotic and biotic degradation of cDCE and VC occurs here.

6. Perspectives on Røddekro plume evolution

The removal of the majority of the source in 2006 has still not resulted in detachment of the plume in Røddekro, as was also documented in 2014. While the plume is growing in the longitudinal direction, it is at a very slow rate; natural destructive processes are currently able to compensate for chlorinated ethene transport in the aquifer and the plume has remained at more or less steady state after the remediation event. However, the aquifer redox conditions, which were altered by the DOC release, are returning to their natural state prior to the source remediation.

The microbial response to the DOC release from the thermal remediation indicates that if remediation were to be applied to the plume, it would be a good candidate for biostimulation. Furthermore, the relatively high pore water velocity would ensure quick, widespread donor distribution. Nevertheless, the DOC concentrations in the wells immediately downgradient from the source still match the levels recorded in 2014 and there is more evidence of biotic degradation than in previous sampling campaigns. The degree to which the destructive processes occur is sufficient to contain the contamination and remediation is not necessary at present. This is fortunate, as despite the positive microbial response to the DOC release, a plume of such depth and extent is still difficult to remediate, and monitored natural attenuation is a

more efficient use of resources.

While the future of the plume is impossible to foretell, based on the response to the remediation event over the past decade, it is likely that the natural attenuation processes in the plume will be sustained for some time in the future. The reduced conditions in the plume required substantial input to change, but appear to be sustained longer than was originally predicted. This may be due to further production of electron donor, hydrogen, from fermentation of endogenous biomass decay products as the activity of the microbial community decreases (Adamson and Newell, 2009; Sleep et al., 2005). Monitored natural attenuation in the plume will likely remain a sufficient approach considering that some biotic degradation was documented to occur prior to the remediation event and that, post remediation, there is much less contaminant mass entering the plume. The long-term evaluation of the plume response to the source remediation event gives a broader perspective to management of the risk posed by contaminated sites.

7. Conclusion

Continued, in-depth study of the Røddekro plume has produced an extensive dataset from multiple lines of evidence that encompasses more than a decade of plume evolution. This dataset allows for a unique, deep dive into the processes and degradation mechanisms that impact the fate and transport of the chlorinated ethenes. The various scales and scopes of the site investigation allow for us to not only make conclusions about the plume as a whole, but also to investigate processes on a smaller scale and over time. For example, the delayed response to the 2014 redox changes can be identified by the appearance of quantifiable amounts of bacteria and *rdhA* genes in 2017. The estimation of local degradation rates yields information about the fate of the contaminants and also adds to the library of degradation rates available in the literature for risk assessment (Ottosen et al., 2019). Furthermore, the dataset provides the opportunity to reassess old data with new knowledge, such as estimation of degradation rates, dual C-Cl isotope slopes, and discovery of new *rdhA* genes.

However, there are still limitations to what can be achieved with the extensive dataset. The lines of evidence approach is successful for definite identification that the chlorinated ethenes undergo a destructive process, but when two lines of evidence indicate different mechanisms, it is still problematic to ascertain the distinct mechanism(s) responsible for the contaminant degradation. As was discussed in Badin et al., 2016, sites with complex iron geochemistry are not well explored. More research on these systems could further our understanding of the interplay between biotic and abiotic degradation. Additionally, the field of dual C-Cl isotope analysis is relatively new and is still evolving, as Cl isotope analysis has only become more reliable in recent years (Elsner et al., 2012). While dual C-Cl isotope slopes can provide valuable information in the assessment of which degradation mechanism(s) occur, further research is required to combine slope trends and degradation by specific bacteria strains, and to evaluate how simultaneously occurring degradation pathways influence these trends.

The extensive temporal and spatial analysis of the Røddekro plume allows for tracking the evolution of the plume and the lasting impact of the source remediation. The plume itself is complex throughout its length, and the multiple lines of evidence approach is essential to elucidate the primary degradation mechanisms in its various areas. Each line of evidence can be used to strengthen the others, and the information they give in combination is greater than the sum of their parts.

Acknowledgements

We gratefully acknowledge the Region of Southern Denmark, Denmark for the opportunity to sample at the site and for partial financing of the sampling campaign. Arwos, Denmark is acknowledged for the remainder of the funding for the sampling campaign. DTU is

acknowledged for PhD student funding. We further acknowledge Lone Dissing (Region of Southern Denmark) for feedback on the manuscript and Lone Dissing and Niels Just (Region of Southern Denmark) for their contributions to planning and executing the campaign. Jesper L. Gregersen and Bjarke Foss (Region of Southern Denmark) are acknowledged for their hard work in the field. Aikaterini Tsitonaki (Orbicon) is acknowledged for her feedback on the manuscript, and Aikaterini Tsitonaki and Kresten Andersen (Orbicon) are acknowledged for their involvement in preparing and executing the sampling campaign. Aline Adler and Emmanuelle Rohrbach (EPFL) are acknowledged for their work with sequencing and bioinformatics. Britta Drude (DTU) is acknowledged for her hard work in the field and laboratory and for her contributions to the data treatment and analysis in her MSc project. Lastly, we acknowledge two anonymous reviewers for their constructive comments and help improving the quality of the manuscript.

Appendix A. Supplementary data

Supplementary data to this article can be found online at <https://doi.org/10.1016/j.jconhyd.2019.103551>.

References

- Abe, Y., Hunkeler, D., 2006. Does the Rayleigh equation apply to evaluate field isotope data in contaminant hydrogeology? *Environ. Sci. Technol.* 40, 1588–1596. <https://doi.org/10.1021/es051128p>.
- Abe, Y., Aravena, R., Zopfi, J., Shouakar-Stash, O., Cox, E., Roberts, J.D., Hunkeler, D., 2009. Carbon and chlorine isotope fractionation during aerobic oxidation and reductive dechlorination of vinyl chloride and *cis*-1, 2-dichloroethene. *Environ. Sci. Technol.* 43, 101–107. <https://doi.org/10.1021/es801759k>.
- Adamson, D.T., Newell, C.J., 2009. Support of source zone bioremediation through endogenous biomass decay and electron donor recycling. *Bioremediat. J.* 13, 29–40. <https://doi.org/10.1080/10889860802690539>.
- Aeppli, C., Hofstetter, T.B., Amaral, H.I.F., Kipfer, R., Schwarzenbach, R.P., Berg, M., 2010. Quantifying in situ transformation rates of chlorinated ethenes by combining compound-specific stable isotope analysis, groundwater dating, and carbon isotope mass balances. *Environ. Sci. Technol.* 44, 3705–3711.
- Appelo, C.A.J., Postma, D., 2005. *3 Flow and Transport. Geochemistry, Groundwater and Pollution*, 2nd. CRC Press, pp. 63–118.
- Audf-Miró, C., Cretnik, S., Otero, N., Palau, J., Shouakar-Stash, O., Soler, A., Elsner, M., 2013. Cl and C isotope analysis to assess the effectiveness of chlorinated ethene degradation by zero-valent iron: evidence from dual element and product isotope values. *Appl. Geochem.* 32, 175–183. <https://doi.org/10.1016/j.apgeochem.2012.08.025>.
- Audf-Miró, C., Cretnik, S., Torrentó, C., Rosell, M., Shouakar-Stash, O., Otero, N., Palau, J., Elsner, M., Soler, A., 2015. C, Cl and H compound-specific isotope analysis to assess natural versus Fe(0) barrier-induced degradation of chlorinated ethenes at a contaminated site. *J. Hazard. Mater.* 299, 747–754. <https://doi.org/10.1016/j.jhazmat.2015.06.052>.
- Badin, A., Buttet, G., Maillard, J., Holliger, C., Hunkeler, D., 2014. Multiple dual C-cl isotope patterns associated with reductive dechlorination of tetrachloroethene. *Environ. Sci. Technol.* 48, 9179–9186. <https://doi.org/10.1021/es508822d>.
- Badin, A., Broholm, M.M., Jacobsen, C.S., Palau, J., Dennis, P., Hunkeler, D., 2016. Identification of abiotic and biotic reductive dechlorination in a chlorinated ethene plume after thermal source remediation by means of isotopic and molecular biology tools. *J. Contam. Hydrol.* 192, 1–19. <https://doi.org/10.1016/j.jconhyd.2016.05.003>.
- Bælum, J., Chambon, J.C., Scheutz, C., Binning, P.J., Laier, T., Bjerg, P.L., Jacobsen, C.S., 2013. A conceptual model linking functional gene expression and reductive dechlorination rates of chlorinated ethenes in clay rich groundwater sediment. *Water Res.* 47, 2467–2478. <https://doi.org/10.1016/j.watres.2013.02.016>.
- Berggren, D.R.V., Marshall, I.P.G., Azizian, M.F., Spormann, A.M., Semprini, L., 2013. Effects of sulfate reduction on the bacterial community and kinetic parameters of a dechlorinating culture under chemostat growth conditions. *Environ. Sci. Technol.* 47, 1879–1886. <https://doi.org/10.1021/es304244z>.
- Blazquez-Pali, N., Rosell, M., Varias, J., Bosch, M., Soler, A., Vicent, T., Marco-Urrea, E., et al., 2019. Multi-method assessment of the intrinsic biodegradation potential of an aquifer contaminated with chlorinated ethenes at an industrial area in Barcelona (Spain). *Environmental Pollution* 244, 165–173. <https://doi.org/10.1016/j.envpol.2018.10.013>.
- Bloom, Y., Aravena, R., Hunkeler, D., Edwards, E., Frappe, S.K., 2000. Carbon isotope fractionation during microbial dechlorination of trichloroethene, *cis*-1,2-dichloroethene, and vinyl chloride: implications for assessment of natural attenuation. *Environ. Sci. Technol.* 34, 2768–2772. <https://doi.org/10.1021/es991179k>.
- Bradley, P.M., 2000. Microbial degradation of chloroethenes in groundwater systems. *Hydrogeol. J.* 8, 104–111. <https://doi.org/10.1007/s100400050011>.
- Bradley, P.M., Chapelle, F.H., 2000. Aerobic microbial mineralization of dichloroethene as sole carbon substrate. *Environ. Sci. Technol.* 34, 221–223. <https://doi.org/10.1021/es990785c>.
- Bradley, P.M., Chapelle, F.H., Lovley, D.R., 1998. Humic acids as electron acceptors for anaerobic microbial oxidation of vinyl chloride and dichloroethene. *Appl. Environ. Microbiol.* 64, 3102–3105.
- Braeckvelt, M., Fischer, A., Kästner, M., 2012. Field applicability of Compound-Specific Isotope Analysis (CSIA) for characterization and quantification of in situ contaminant degradation in aquifers. *Appl. Microbiol. Biotechnol.* 94, 1401–1421. <https://doi.org/10.1007/s00253-012-4077-1>.
- Buchner, D., Behrens, S., Laskov, C., Haderlein, S.B., 2015. Resiliency of stable isotope fractionation ($\delta^{13}C$ and $\delta^{37}Cl$) of trichloroethene to bacterial growth physiology and expression of key enzymes. *Environ. Sci. Technol.* 49, 13230–13237. <https://doi.org/10.1021/acs.est.5b02918>.
- Castro, H.F., Williams, N.H., Ogram, A., 2000. Phylogeny of sulfate-reducing bacteria 1. *FEMS Microbiol. Ecol.* 31.
- Courbet, C., Rivière, A., Jeannotat, S., Rinaldi, S., Hunkeler, D., Bendjoudi, H., De Marsily, G., 2011. Complementing approaches to demonstrate chlorinated solvent biodegradation in a complex pollution plume: mass balance, PCR and compound-specific stable isotope analysis. *J. Contam. Hydrol.* 126, 315–329. <https://doi.org/10.1016/j.jconhyd.2011.08.009>.
- Cretnik, S., Thoreson, K., Bernstein, A., Ebert, K., Buchner, D., Laskov, C., Haderlein, S., Shouakar-Stash, O., Kliegman, S., McNeill, K., Elsner, M., 2013. Reductive dechlorination of TCE by chemical model systems in comparison to dehalogenating bacteria: insights from dual element isotope analysis ($^{13}C/^{12}C$, $^{37}Cl/^{35}Cl$). *Environ. Sci. Technol.* 47, 6855–6863. <https://doi.org/10.1021/es400107n>.
- Cretnik, S., Bernstein, A., Shouakar-stash, O., Löffler, F., Elsner, M., 2014. Chlorine isotope effects from isotope ratio mass spectrometry suggest intramolecular C-Cl bond competition in trichloroethene (TCE) reductive dehalogenation. *Molecules* 6450–6473. <https://doi.org/10.3390/molecules19056450>.
- Culpepper, J.D., Scherer, M.M., Robinson, T.C., Neumann, A., Cwiertyny, D., Latta, D.E., 2018. Reduction of PCE and TCE by magnetite revisited. *Environ. Sci. Process. Impacts* 20, 1299–1490. <https://doi.org/10.1039/c8em00286j>.
- Cwiertyny, D.M., Scherer, M.M., 2010. Chapter 2: Chlorinated solvent chemistry: Structures, nomenclature, and properties. In: *In Situ Remediation of Chlorinated Solvent Plumes*, pp. 29–38. <https://doi.org/10.1007/978-1-4419-1401-9>.
- Damgaard, I., Bjerg, P.L., Bælum, J., Scheutz, C., Hunkeler, D., Jacobsen, C.S., Tuxen, N., Broholm, M.M., 2013. Identification of chlorinated solvents degradation zones in clay till by high resolution chemical, microbial and compound specific isotope analysis. *J. Contam. Hydrol.* 146, 37–50. <https://doi.org/10.1016/j.jconhyd.2012.11.010>.
- Doğan-Subaşı, E., Elsner, M., Qiu, S., Cretnik, S., Atashgahi, S., Shouakar-Stash, O., Boon, N., Dejonghe, W., Bastiaens, L., 2017. Contrasting dual (C, Cl) isotope fractionation offers potential to distinguish reductive chloroethene transformation from breakdown by permanganate. *Sci. Total Environ.* 596–597, 169–177. <https://doi.org/10.1016/j.scitotenv.2017.03.292>.
- Elsner, M., Chartrand, M., Vanstone, N., Couloume, G.L., Lollar, B.S., 2008. Identifying abiotic chlorinated ethene degradation: characteristic isotope patterns in reaction products with nanoscale zero-valent iron. *Environ. Sci. Technol.* 42, 5963–5970. <https://doi.org/10.1021/es8001986>.
- Elsner, M., Jochmann, M.A., Hofstetter, T.B., Hunkeler, D., Bernstein, A., Schmidt, T.C., Schimmelmann, A., 2012. Current challenges in compound-specific stable isotope analysis of environmental organic contaminants. *Anal. Bioanal. Chem.* 403, 2471–2491. <https://doi.org/10.1007/s00216-011-5683-y>.
- Friis, A.K., Albrechtsen, H.J., Heron, G., Bjerg, P.L., 2005. Redox processes and release of organic matter after thermal treatment of a TCE-contaminated aquifer. *Environ. Sci. Technol.* 39, 5787–5795.
- Gafni, A., Lihl, C., Gelman, F., Elsner, M., Bernstein, A., 2018. $\delta^{13}C$ and $\delta^{37}Cl$ isotope fractionation to characterize aerobic vs anaerobic degradation of trichloroethylene. *Environ. Sci. Technol. Lett.* 5, 202–208. <https://doi.org/10.1021/acs.estlett.8b00100>.
- Gossett, J.M., 2010. Sustained aerobic oxidation of vinyl chloride at low oxygen concentrations. *Environ. Sci. Technol.* 44, 1405–1411.
- Griebler, C., Lueders, T., Mu, H.Z., 2009. Microbial Biodiversity in Groundwater Ecosystems. pp. 649–677. <https://doi.org/10.1111/j.1365-2427.2008.02013.x>.
- Harkness, M., Fisher, A., Lee, M.D., MacK, E.E., Payne, J.A., Dworatzek, S., Roberts, J., Acheson, C., Herrmann, R., Possolo, A., 2012. Use of statistical tools to evaluate the reductive dechlorination of high levels of TCE in microcosm studies. *J. Contam. Hydrol.* 131, 100–118. <https://doi.org/10.1016/j.jconhyd.2012.01.011>.
- He, Y.T., Wilson, J.T., Wilkin, R.T., 2015. Review of abiotic degradation of chlorinated solvents by reactive iron minerals in aquifers. *Groundw. Monit. Remediat.* 35, 57–75. <https://doi.org/10.1111/gwmr.12111>.
- Holliger, C., Schraa, G., Stams, A.J.M., Zehnder, A.J.B., 1993. A highly purified enrichment culture couples the reductive dechlorination of tetrachloroethene to growth. *Appl. Environ. Microbiol.* 59, 2991–2997.
- Hug, L.A., Beiko, R.G., Rowe, A.R., Richardson, R.E., Edwards, E.A., 2012. Comparative metagenomics of three *Dehalococcoides*-containing enrichment cultures: the role of the non-dechlorinating community. *BMC Genomics* 13. <https://doi.org/10.1186/1471-2164-13-327>.
- Hug, L. a, Maphosa, F., Leys, D., Löffler, F.E., Smidt, H., Edwards, E. a, Adrian, L., 2013. Overview of organohalide-respiring bacteria and a proposal for a classification system for reductive dehalogenases. *Philos. Trans. R. Soc. Lond. Ser. B Biol. Sci.* <https://doi.org/10.1098/rstb.2012.0322>.
- Hunkeler, D., Van Breukelen, B.M., Elsner, M., 2009. Modeling chlorine isotope trends during sequential transformation of chlorinated ethenes. *Environ. Sci. Technol.* 43, 6750–6756. <https://doi.org/10.1021/es900579z>.
- Hunkeler, D., Abe, Y., Broholm, M.M., Jeannotat, S., Westergaard, C., Jacobsen, C.S., Aravena, R., Bjerg, P.L., 2011. Assessing chlorinated ethene degradation in a large scale contaminant plume by dual carbon-chlorine isotope analysis and quantitative PCR. *J. Contam. Hydrol.* 119, 69–79. <https://doi.org/10.1016/j.jconhyd.2010.09.009>.
- Hyun, S.P., Hayes, K.F., 2015. Abiotic reductive dechlorination of *cis*-DCE by ferrous monosulfide mackinawite. *Environ. Sci. Pollut. Res.* 22, 16463–16474. <https://doi.org/10.1007/s11356-015-5033-2>.
- Imfeld, G., Nijenhuis, I., Nikolaus, M., Zeiger, S., Paschke, H., Drangmeister, J., Grossmann, J., Richnow, H.H., Weber, S., 2008. Assessment of in situ degradation of chlorinated ethenes and bacterial community structure in a complex contaminated

- groundwater system. *Water Res.* 42, 871–882. <https://doi.org/10.1016/j.watres.2007.08.035>.
- Imfeld, G., Aragonés, C.E., Fetzer, I., Mészáros, É., Zeiger, S., Nijenhuis, I., Nikolausz, M., Delerce, S., Richnow, H.H., 2010. Characterization of microbial communities in the aqueous phase of a constructed model wetland treating 1,2-dichloroethene-contaminated groundwater. *FEMS Microbiol. Ecol.* 72, 74–88. <https://doi.org/10.1111/j.1574-6941.2009.00825.x>.
- Imfeld, G., Pieper, H., Shani, N., Rossi, P., Nikolausz, M., Nijenhuis, I., Paschke, H., Weiss, H., Richnow, H.H., 2011. Characterization of groundwater microbial communities, dechlorinating bacteria, and in situ biodegradation of chloroethenes along a vertical gradient. *Water Air Soil Pollut.* 221, 107–122. <https://doi.org/10.1007/s11270-011-0774-0>.
- Jeong, H.Y., Anantharaman, K., Han, Y.S., Hayes, K.F., 2011. Abiotic reductive dechlorination of *cis*-dichloroethylene by Fe species formed during iron- or sulfate-reduction. *Environ. Sci. Technol.* 45, 5186–5194. <https://doi.org/10.1021/es104387w>.
- Kret, E., Kiecak, A., Malina, G., Nijenhuis, I., Postawa, A., 2015. Identification of TCE and PCE sorption and biodegradation parameters in a sandy aquifer for fate and transport modelling: batch and column studies. *Environ. Sci. Pollut. Res.* 22, 9877–9888. <https://doi.org/10.1007/s11356-015-4156-9>.
- Kuder, T., Van Breukelen, B.M., Vanderford, M., Philp, P., 2013. 3D-CSIA: carbon, chlorine, and hydrogen isotope fractionation in transformation of TCE to ethene by a *Dehalococcoides* culture. *Environ. Sci. Technol.* 47, 9668–9677. <https://doi.org/10.1021/es400463p>.
- Lee, W., Batchelor, B., 2002a. Abiotic reductive dechlorination of chlorinated ethylenes by iron-bearing soil minerals. 1. Pyrite and magnetite. *Environ. Sci. Technol.* 36, 5147–5154.
- Lee, W., Batchelor, B., 2002b. Abiotic reductive dechlorination of chlorinated ethylenes by iron-bearing soil minerals. 2. Green rust. *Environ. Sci. Technol.* 36, 5348–5354. <https://doi.org/10.1021/es025837a>.
- Liang, X., Paul Philp, R., Butler, E.C., 2009. Kinetic and isotope analyses of tetrachloroethylene and trichloroethylene degradation by model Fe(II)-bearing minerals. *Chemosphere* 75, 63–69. <https://doi.org/10.1016/j.chemosphere.2008.11.042>.
- Liang, Y., Liu, X., Singletary, M.A., Wang, K., Mattes, T.E., 2017. Relationships between the abundance and expression of functional genes from vinyl chloride (VC)-degrading bacteria and geochemical parameters at VC-contaminated sites. *Environ. Sci. Technol.* 51, 12164–12174. <https://doi.org/10.1021/acs.est.7b03521>.
- Lihl, C., Douglas, L.M., Franke, S., Perez-de-Mora, A., Meyer, A.H., Daubmeier, M., Edwards, E.A., Nijenhuis, I., Lollar, B.S., Elsner, M., 2019. Mechanistic dichotomy in bacterial trichloroethene dechlorination revealed by carbon and chlorine isotope effects. *Environ. Sci. Technol.* 53, 4245–4254. <https://doi.org/10.1021/acs.est.8b06643>.
- Löffler, F.E., Yan, J., Ritalahti, K.M., Adrian, L., Edwards, E.A., Konstantinidis, K.T., Müller, J.A., Fullerton, H., Zinder, S.H., Spormann, A.M., 2013. *Dehalococcoides mccartyi* gen. nov., sp. nov., obligately organohalide-respiring anaerobic bacteria relevant to halogen cycling and bioremediation, belong to a novel bacterial class, *Dehalococcoidia classis* nov., order *Dehalococcoidales* ord. nov. *Int. J. Syst. Evol. Microbiol.* 63, 625–635. <https://doi.org/10.1099/ijse.0.034926-0>.
- Lollar, B.S., Slater, G.F., Sleep, B., Witt, M., Klecka, G.M., Harness, M., Spivack, J., 2001. Stable carbon isotope evidence for intrinsic bioremediation of tetrachloroethene and trichloroethene at Area 6, Dover Air Force Base. *Environ. Sci. Technol.* 35, 261–269. <https://doi.org/10.1021/es001227x>.
- Maphosa, F., de Vos, W.M., Smidt, H., 2010. Exploiting the ecogenomics toolbox for environmental diagnostics of organohalide-respiring bacteria. *Trends Biotechnol.* 28, 308–316. <https://doi.org/10.1016/j.tibtech.2010.03.005>.
- McDonald, D., Price, M.N., Goodrich, J., Nawrocki, E.P., Desantis, T.Z., Probst, A., Andersen, G.L., Knight, R., Hugenholtz, P., 2012. An improved GreenGenes taxonomy with explicit ranks for ecological and evolutionary analyses of bacteria and archaea. *ISME J.* 6, 610–618. <https://doi.org/10.1038/ismej.2011.139>.
- Morrill, P.L., Lacrampe-Couloume, G., Slater, G.F., Sleep, B.E., Edwards, E.A., McMaster, M.L., Major, D.W., Lollar, B.S., 2005. Quantifying chlorinated ethene degradation during reductive dechlorination at Kelly AFB using stable carbon isotopes. *J. Contam. Hydrol.* 76, 279–293. <https://doi.org/10.1016/j.jconhyd.2004.11.002>.
- Murray, A.M., 2019. Impact of the Microbial Community on Chlorinated Ethene Degradation: Laboratory, Modeling, and Field Investigation. Technical University of Denmark.
- Murray, A., Maillard, J., Jin, B., Broholm, M., Holliger, C., Rolle, M., 2019. A modeling approach integrating microbial activity, mass transfer, and geochemical processes to interpret biological assays: an example for PCE degradation in a multi-phase batch setup (under review). *Water Res.* 160, 484–496. <https://doi.org/10.1016/j.watres.2019.05.087>.
- Nawrocki, E.P., Eddy, S.R., 2013. Infernal 1.1: 100-fold faster RNA homology searches. *Bioinformatics* 29, 2933–2935. <https://doi.org/10.1093/bioinformatics/btt509>.
- Nazaroff, W.W., Alvarez-Cohen, L., 2001. *Environmental Engineering Science*. John Wiley & Sons.
- Nijenhuis, I., Nikolausz, M., Koth, A., Felföldi, T., Weiss, H., Drangmeister, J., Großmann, J., Kastner, M., Richnow, H., 2007. Assessment of the natural attenuation of chlorinated ethenes in an anaerobic contaminated aquifer in the Bitterfeld/Wolfen area using stable isotope techniques, microcosm studies and molecular biomarkers. *Chemos* 67, 300–311. <https://doi.org/10.1016/j.chemosphere.2006.09.084>.
- Nijenhuis, I., Stollberg, R., Lechner, U., 2018. Anaerobic microbial dehalogenation and its key players in the contaminated Bitterfeld-Wolfen megasite. *FEMS Microbiol. Ecol.* 94. <https://doi.org/10.1093/femsec/fiy012>.
- Ottosen, C.B., Murray, A.M., Broholm, M.M., Bjerg, P.L., 2019. In situ quantification of degradation is needed for reliable risk assessments and site-specific monitored natural attenuation. *Environ. Sci. Technol.* 53, 1–3. <https://doi.org/10.1021/acs.est.8b06630>.
- Paes, F., Liu, X., Mattes, T.E., Cupples, A.M., 2015. Elucidating carbon uptake from vinyl chloride using stable isotope probing and illumina sequencing. *Appl. Microbiol. Biotechnol.* 99, 7735–7743. <https://doi.org/10.1007/s00253-015-6606-1>.
- Pérez-De-Mora, A., Zila, A., McMaster, M.L., Edwards, E., 2014. Bioremediation of chlorinated ethenes in fractured bedrock and associated changes in dechlorinating and nondechlorinating microbial populations. *Environ. Sci. Technol.* 48, 5770–5779. <https://doi.org/10.1021/es404122y>.
- Richards, P.M., Liang, Y., Johnson, R.L., Mattes, T.E., 2019. Cryogenic soil coring reveals coexistence of aerobic and anaerobic vinyl chloride degrading bacteria in a chlorinated ethene contaminated aquifer. *Water Res.* 157, 281–291. <https://doi.org/10.1016/j.watres.2019.03.059>.
- Ritalahti, K.M., Amos, B.K., Sung, Y., Wu, Q., Koenigsberg, S.S., Löffler, F.E., 2006. Quantitative PCR targeting 16S rRNA and reductive dehalogenase genes simultaneously monitors multiple *Dehalococcoides* strains. *Appl. Environ. Microbiol.* 72, 2765–2774. <https://doi.org/10.1128/AEM.72.4.2765-2774.2006>.
- Robertson, W.J., Bowman, J.P., Franzmann, P.D., Mee, B.J., 2001. *Desulfosporosinus meridiei* sp. nov., a spore-forming sulfate-reducing bacterium isolated from gasoline-contaminated groundwater. *Int. J. Syst. Evol. Microbiol.* 51, 133–140.
- Scheutz, C., Broholm, M.M., Durant, N.D., Weeth, E.B., Jørgensen, T.H., Dennis, P., Jacobsen, C.S., Cox, E.E., Chambon, J.C., Bjerg, P.L., 2010. Field evaluation of biological enhanced reductive dechlorination of chloroethenes in clayey till. *Environ. Sci. Technol.* 44, 5134–5141. <https://doi.org/10.1021/es1003044>.
- Schippers, A., Jørgensen, B.B., 2002. Biogeochemistry of pyrite and iron sulfide oxidation in marine sediments. *Geochim. Cosmochim. Acta* 66, 85–92. [https://doi.org/10.1016/S0016-7037\(01\)00745-1](https://doi.org/10.1016/S0016-7037(01)00745-1).
- Shani, N., Rossi, P., Holliger, C., 2013. Correlations between environmental variables and bacterial community structures suggest Fe(III) and vinyl chloride reduction as antagonistic terminal electron-accepting processes. *Environ. Sci. Technol.* 47, 6836–6845. <https://doi.org/10.1021/es304017s>.
- Silverman, M.P., 1967. Mechanism of bacterial pyrite oxidation. *J. Bacteriol.* 94, 1046–1051.
- Sleep, B.E., Brown, A.J., Lollar, B.S., 2005. Long-term tetrachloroethene degradation sustained by endogenous cell decay. *J. Environ. Eng. Sci.* 4, 11–17. <https://doi.org/10.1139/s04-038>.
- Smits, T.H.M., Assal, A., Hunkeler, D., Holliger, C., 2011. Anaerobic degradation of vinyl chloride in aquifer microcosms. *J. Environ. Qual.* 40, 915. <https://doi.org/10.2134/jeq2010.0403>.
- Theis, C.V., 1935. The relation between the lowering of the Piezometric surface and the rate and duration of discharge of a well using groundwater storage. *Trans. Am. Geophys. Union* 16, 519–524.
- Thullner, M., Centler, F., Richnow, H., Fischer, A., 2012. Organic Geochemistry Quantification of organic pollutant degradation in contaminated aquifers using compound specific stable isotope analysis – review of recent developments. *Org. Geochem.* 42, 1440–1460. <https://doi.org/10.1016/j.orggeochem.2011.10.011>.
- Vanstone, N.A., Focht, R.M., Mabury, S.A., Sherwood Lollar, B., 2004. Effect of iron type on kinetics and carbon isotopic enrichment of chlorinated ethylenes during abiotic reduction on Fe(O). *Ground Water*. <https://doi.org/10.1111/j.1745-6584.2004.tb02673.x>.
- Wang, P.H., Correia, K., Ho, H.C., Venayak, N., Nemr, K., Flick, R., Mahadevan, R., Edwards, E.A., 2019. An interspecies malate-pyruvate shuttle reconciles redox imbalance in an anaerobic microbial community. *ISME J.* <https://doi.org/10.1038/s41396-018-0333-4>.
- Weber, K.A., Achenbach, L.A., Coates, J.D., 2006. Microorganisms pumping iron: anaerobic microbial iron oxidation and reduction. *Nat. Rev. Microbiol.* 4, 752–764. <https://doi.org/10.1038/nrmicro1490>.
- Wiegert, C., Aeppli, C., Knowles, T., Holmstrand, H., Evershed, R., Pancost, R.D., Macháčkova, J., Gustafsson, Ö., 2012. Dual carbon-chlorine stable isotope investigation of sources and fate of chlorinated ethenes in contaminated groundwater. *Environ. Sci. Technol.* 46, 10918–10925. <https://doi.org/10.1021/es3016843>.
- Wiegert, C., Mandalakis, M., Knowles, T., Polymenakou, P.N., Aeppli, C., Macháčkova, J., Holmstrand, H., Evershed, R.P., Pancost, R.D., Gustafsson, Ö., Gustafsson, Ö., 2013. Carbon and chlorine isotope fractionation during microbial degradation of tetra- and trichloroethene. *Environ. Sci. Technol.* 47, 6449–6456. <https://doi.org/10.1021/es305236y>.
- Wilson, J.T., 2010. Monitored natural attenuation of chlorinated solvent plumes. In: Stroo, H.F., Ward, C.H. (Eds.), *In Situ Remediation of Chlorinated Solvent Plumes*. Springer Science + Business Media, pp. 325–355.
- Yang, Y., Higgins, S.A., Yan, J., Şimşir, B., Chourey, K., Iyer, R., Hettich, R.L., Baldwin, B., Ogles, D.M., Löffler, F.E., 2017. Grape pomace compost harbors organohalide-respiring *Dehalogenimonas* species with novel reductive dehalogenase genes. *ISME J.* 2767–2780. <https://doi.org/10.1038/ismej.2017.127>.
- Yargicoglu, E.N., Reddy, K.R., 2015. Review of biological diagnostic tools and their applications in geoenvironmental engineering. *Rev. Environ. Sci. Biotechnol.* 14, 161–194. <https://doi.org/10.1007/s11157-014-9358-y>.
- Yarza, P., Yilmaz, P., Pruesse, E., Glöckner, F.O., Ludwig, W., Schleifer, K.H., Whitman, W.B., Euzéby, J., Amann, R., Rosselló-Móra, R., 2014. Uniting the classification of cultured and uncultured bacteria and archaea using 16S rRNA gene sequences. *Nat. Rev. Microbiol.* 12, 635–645. <https://doi.org/10.1038/nrmicro3330>.
- Zhang, J., Kobert, K., Flouri, T., Stamatakis, A., 2014. PEAR: a fast and accurate Illumina Paired-End reAd mergeR. *Bioinformatics* 30, 614–620. <https://doi.org/10.1093/bioinformatics/btt593>.